Universitat Politècnica de Catalunya

Experimental study of speckle generated by semiconductor light sources: application in double pass imaging

A thesis submitted by

Donatus Halpaap

in fulfillment of the requirements of the degree of
Doctor in Computational and Applied Physics

Directors:
Cristina Masoller
Meritxell Vilaseca Ricart

Departament de Física
Terrassa, October 2019

Abstract

Experimental study of speckle generated by semiconductor light sources: application in double pass imaging

With the double pass (DP) technique it is possible to quantify the optical quality of a patient's eye by measuring its point spread function. Due to the low reflectivity of the retina a high-intensity, point-like illumination source is required. Usually laser diodes (LDs) are used, but the coherent laser light produces speckle, an interference phenomenon that deteriorates image quality and can make DP images difficult or impossible to interpret. A low-cost solution to reduce speckle in DP imaging is to include a vibrating mirror in the optical path of the system and average over the different speckle realizations. However, vibrating mechanical parts are undesired because they limit longevity and reliability of medical equipment.

The goal of this thesis is to find an inexpensive non-mechanical solution for speckle reduction in DP imaging based on low-coherence semiconductor light sources. We compare an LD, a light-emitting diode (LED) and a superluminescent diode (SLED) in terms of speckle formation, cost and usability in DP systems. We find that the SLED is a good alternative to LD illumination, as the amount of speckle in the image is almost as low as that obtained with an LD and a vibrating mirror in the beam path. However, the SLED is not a low-cost solution. In order to identify a cost-efficient all-optical solution, we analyze the speckle generated by an LD as a function of its pump current. Our experiments suggest that driving the LD below the lasing threshold can be an inexpensive solution for speckle reduction. While undesired in many imaging applications, speckle can also contain useful information that is exploited, e.g., in blood flow analysis or for reconstruction of the object that generates the speckle pattern. We find that adjusting the pump current of an LD and the exposure time of the image acquisition system can be a simple and effective way to increase or reduce the amount of speckle by tailoring the coherence of light used for imaging. In particular, we identify conditions that allow to record images with similar average intensity, but with speckle contrast values as low as 0.16, or as high as 0.99.

Resumen

Estudio experimental del speckle generado por fuentes de luz semiconductoras: aplicación en imágenes de doble paso

Con la técnica de doble paso (DP) es posible cuantificar la calidad óptica del ojo de un paciente midiendo la función de dispersión de punto. Debido a la baja reflectividad de la retina, se requiere una fuente de luz puntual de alta intensidad. Una fuente de luz ampliamente utilizada en sistemas de DP son los diodos láser (LD). Los diodos láser son fuentes de luz coherentes que producen patrones de interferencia cuando se ilumina una superficie rugosa. Este fenómeno de interferencia, denominado speckle, deteriora la calidad de la imagen y puede hacer que las imágenes de DP sean difíciles o imposibles de interpretar. Una solución eficaz y de bajo coste para reducir el speckle en las imágenes de DP es incluir un espejo vibratorio en el camino óptico del sistema para promediar sobre las diferentes realizaciones de patrones de speckle. Sin embargo, las partes mecánicas vibratorias no son una solución óptima puesto que limitan la longevidad y fiabilidad de equipos médicos.

El objetivo de esta tesis es encontrar una solución no mecánica de bajo coste para la reducción de speckle en imágenes de DP basada en fuentes de luz semiconductoras de baja coherencia. Comparamos un LD, un diodo emisor de luz (LED) y un diodo superluminiscente (SLED) en términos de formación de speckle, coste y usabilidad en sistemas de DP. Encontramos que el SLED es una buena alternativa a la iluminación con LD, ya que la cantidad de speckle en la imagen es prácticamente la misma que la obtenida con un LD y un espejo vibratorio. Sin embargo, el SLED no es una solución de bajo coste. Con el fin de identificar una solución totalmente óptica y económicamente rentable, analizamos los patrones de speckle generados por un LD en función de su corriente de bombeo. Nuestros experimentos sugieren que trabajar con corrientes por debajo del umbral del láser puede ser una solución económicamente viable para la reducción de speckle. En muchas aplicaciones de *imaging* se intenta evitar el speckle. De todas formas, el patrón de speckle puede contener información útil que se utiliza, por ejemplo, en el análisis del flujo sanguíneo o para la reconstrucción de objetos. Hemos observado que ajustar la corriente de bombeo de un LD (es decir, adaptar la coherencia de la luz utilizada para la toma de imágenes) puede ser una manera simple y efectiva de aumentar o reducir la cantidad de speckle. Para obtener imágenes con la misma intensidad hay que adaptar el tiempo de exposición del sistema de adquisición de imágenes. En particular, identificamos condiciones que permiten adquirir imágenes con una intensidad mediana similar, pero con valores de *contraste de speckle* que varían entre 0,16 y 0,99.

Resum

Estudi experimental de l'speckle generat per fonts de llum semiconductores: aplicació en imatges de doble pas

Amb la tècnica de doble pas (DP) és possible quantificar la qualitat òptica de l'ull d'un pacient mesurant la funció de dispersió de punt. A causa de la baixa reflectivitat de la retina, es requereix una font de llum puntual d'alta intensitat. Una font de llum ampliament utilitzada en sistemes de DP són els díodes làser (LD). Els díodes làser són fonts de llum coherents que produeixen patrons d'interferència quan s'il·lumina una superficie rugosa. Aquest fenomen d'interferència, anomenat speckle, deteriora la qualitat de la imatge i pot fer que les imatges de DP siguin difícils o impossibles d'interpretar. Una solució eficaç i de baix cost per a reduir l'speckle en les imatges de DP és incloure un mirall vibratori en el camí òptic del sistema per tal de fer la mitjana sobre les diferents realitzacions de patrons d'speckle. No obstant, les parts mecàniques vibratòries no són una solució òptima ja que limiten la longevitat i fiabilitat d'equips mèdics.

L'objectiu d'aquesta tesi és trobar una solució no mecànica de baix cost per a la reducció d'speckle en imatges de DP basada en fonts de llum semiconductores de baixa coherència. Comparem un LD, un díode emissor de llum (LED) i un díode superluminiscent (SLED) en termes de formació d'speckle, cost i usabilitat en sistemes de DP. Trobem que l'SLED és una bona alternativa a la il·luminació amb LD, ja que la reducció de la quantitat d'speckle en la imatge és pràcticament la mateixa que l'obtinguda amb un LD i un mirall vibratori. Tanmateix, l'SLED no és una solució de baix cost. Amb la finalitat d'identificar una solució totalment òptica i econòmicament rendible, analitzem els patrons d'speckle generats per un LD en funció del seu corrent de bombeig. Els nostres experiments suggereixen que treballar amb corrents per sota del llindar d'encesa del làser pot ser una solució econòmicament viable per a la reducció d'speckle. En moltes aplicacions d'*imaging* s'intenta evitar l'speckle. Tot i així, el patró d'speckle pot contenir informació útil que s'utilitza, per exemple, en l'anàlisi del flux sanguini o per a la reconstrucció d'objectes. Hem observat que ajustar el corrent de bombeig d'un LD (és a dir, adaptar la coherència de la llum utilitzada per a la presa d'imatges) pot ser una manera simple i efectiva d'augmentar o reduir la quantitat d'speckle. Per tal d'obtenir imatges amb la mateixa intensitat cal adaptar el temps d'exposició del sistema d'adquisició d'imatges. En particular, identifiquem condicions que permeten adquirir imatges amb una intensitat mitjana similar, però amb valors de *contrast d'speckle* que varien entre 0,16 i 0,99.

Acknowledgments

This work could not have been done without the support of many people. It is always difficult to mention each one who helped in one or another way but I thank them all.

In particular, I want to thank the directors of my thesis, Cristina Masoller and Meritxell Vilaseca, for accepting me to prepare this work under their guidance. I am thankful for their suggestions and productive discussions.

During a stay at Centre de Nanosciences et de Nanotechnologies (C2N, CNRS), in Marcoussis, France, Alejandro Giacomotti, Mathias Marconi and Romain Hernandez welcomed me. They explained the coupling of nanolasers and superthermal light and conducted experiments on speckle formation from nanolaser light with me.

In the Centre for Sensors, Instruments and Systems Development (CD6), Pau Santos, Joan Martínez, Carlos García, Fernando Díaz and Mikel Aldaba introduced me to double pass imaging and discussed questions with me. Carlos García helped me with experimental and theoretical questions and provided the Matlab code which formed the basis of my double pass image analysis software. Xavier Murcia provided me with mechanical and Fermín Alarcon with electronic solutions for my experiments. Cristina Cusidó, Julia Sebastián and Laura Escolano solved administrative questions with great patience. In Nonlinear Dynamics, Nonlinear Optics and Lasers group (DONLL), Jordi Tiana and Carlos Quintero were guides to me in using laboratory equipment and solving software questions regarding Labview and Matlab. I am grateful to all of them.

I thank my coworkers for creating a nice and fruitful environment. The students Cisco, Shubham, Hossam, Binxia, Waqas, Dario, Clara, Tommaso, Ana, Maria, Pablo, Judith, Sandeep, Laura R.B., Laura R.S., Salim and Riccardo as well as the guest students I shared the office with, Fabián, Concetta and Tetsu are not only colleagues, but also friends. I got to know the professors Ramon Vilaseca, Crina Cojocaru, Ramon Herrero, Muriel Botey, Jaume Pujol, Kestas Staliunas, Toni Pons and Carles Serrat and discussed with them about science and non-scientific things. All of this helped to finish this thesis.

Finally, I acknowledge funding through a Marie Curie grant by the BE-OPTICAL project (H2020-675512) while conducting the work that lead to this thesis.

Contents

List of acronyms

DP	double pass
FWHM	full width half maximum
LD	laser diode
LED	light emitting diode
MPE	maximum permissible exposure
MTF	modulation transfer function
NDF	neutral density filter
OSI	objective scatter index
OTF	optical transfer function
OSA	optical spectrum analyzer
PDF	probability density function
PSF	point spread function
PTF	phase transfer function
SLED	superluminescent light emitting diode
SR	Strehl ratio
VCSEL	vertical-cavity surface-emitting laser

1 Introduction

A lot of research is carried out nowadays with the goal of developing methods and optical instruments to improve diagnosis, follow-up and treatment of ocular diseases [1–3]. As a result, new products are transferred into the clinical practice, improving health and life quality of patients and having an important economic impact. In this thesis we are focusing on double pass imaging, which is one of these methods.

1.1 Double pass imaging

The double pass (DP) imaging technique is a method used in the fields of opthalmology and optometry for the objective evaluation of the overall optical quality of the eye, including ocular aberrations and intraocular scattering in one single measurement [4–11]. It is based on determining the ocular point spread function (PSF, that is the impulse response of the optics) of the eye by imaging the reflection of a point source projected onto the retina as schematically depicted in Fig. 1.1.

The name of the technique is related to the fact that light for measuring travels through the eye twice, once from the outside to the retina and once, after reflection, in reverse direction. Usually, only the intensity of DP images is of interest and they are recorded only as monochrome images. Figure 1.2 shows a typical DP image with the intensity levels marked in color.

In order to accurately determine the PSF of the eye, a DP system requires a point source. Due to the low reflectivity of the retina (see Fig. 1.3 for experimental data on foveal reflectivity at several wavelenghts and Fig. 1.4 for a diagram of the eye), the light source used should also emit sufficiently high power. These two requirements are usually achieved by employing a laser diode (LD) with a spatial filter (e.g. a single-mode fiber) as shown in the sketch of a DP setup in Fig. 1.5. The laser beam is then widened, collimated and cut by a circular entrance pupil (EP) of usually around 2 mm diameter. DP measurements are carried out in conditions where the eye's pupil has a larger diameter than the entrance pupil. Furthermore, slightly above 2 mm entrance pupil diameter, the eye's resolution is the highest. At lower entrance pupil diameters, it is reduced due to diffraction and at higher diameters due to aberrations as shown in Fig. 1.6.

Before the light enters the eye, it passes a Badal system, i.e. two lenses whose distance to each other can be altered (by moving mirrors M2 and M3 in Fig. 1.5), in order to compensate spherical

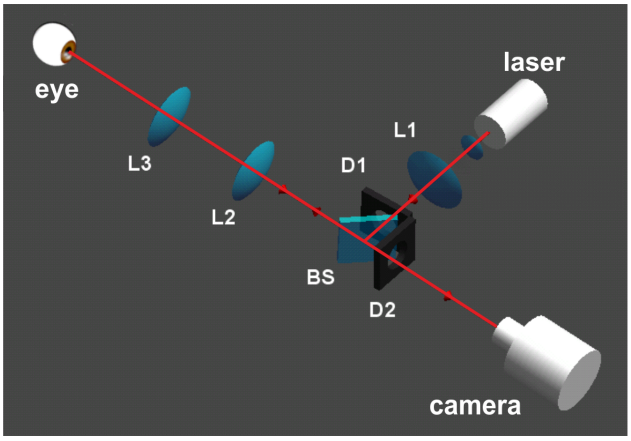

Figure 1.1: Sketch of a double pass (DP) system. L1 - L3: lenses. BS: beam splitter. D1, D2: entrance pupil and exit pupil, respectively. Adapted from lecture notes from M. Vilaseca.

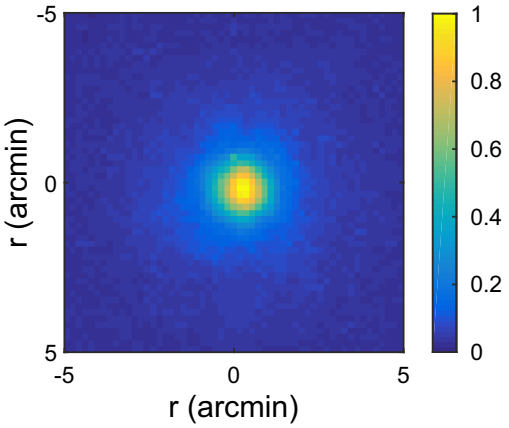

Figure 1.2: Typical DP image. In the originally monochrome image, the intensity levels are colored for clarity.

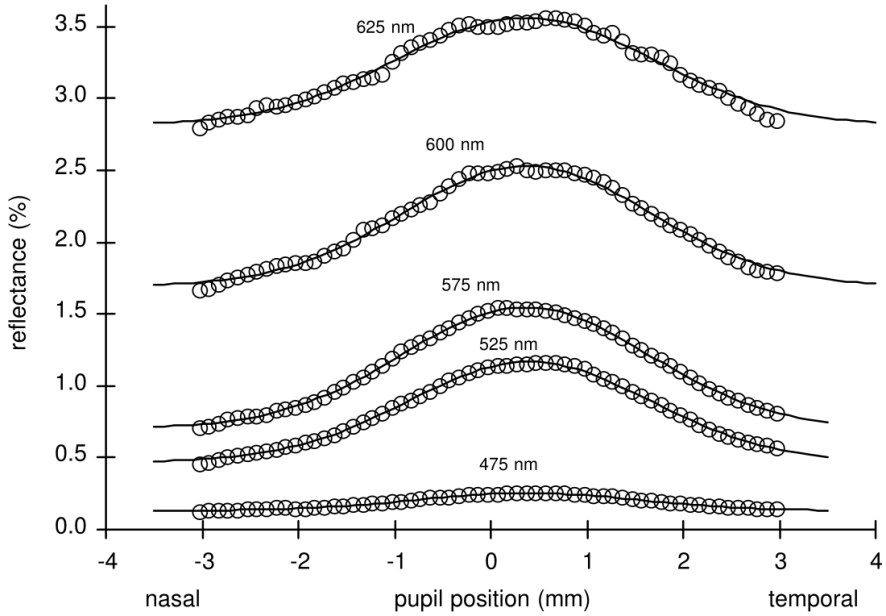

Figure 1.3: Spatial profiles of the foveal reflectance at different wavelengths. The location of the fovea is shown in Fig. 1.4. The reflectance dependence on pupil position is related to the directional sensitivity of the cone photoreceptors ("Stiles–Crawford effect"). Adapted from [12].

refractive errors of the eye. The image of the point source is formed on the retina by the eye's lens. There, it is reflected, and passes in reverse direction through the eye and the Badal system. Then it is coupled out by a beam splitter and passes the exit pupil (ExP, diameter usually around 4 mm), which is, like the entrance pupil, located in a conjugated plane of the eye's pupil. Finally, a camera (CCD1) records the light. The sensor of the camera is in a plane optically conjugated with the retinal plane.

DP imaging can be done at different wavelengths, but for the patient's comfort near-infrared light (780 nm) is preferable. Due to the low sensitivity of the eye at these wavelengths, even bright light is barely noticed. The power arriving at the eye is limited for the patient's safety (see subsection 1.1.4).

1.1.1 Point spread function of the eye

The point spread function describes how an ideal point object is imaged by an imaging system, in our case the eye.

The image formation in DP imaging is described mathematically in [5]. The intensity of the

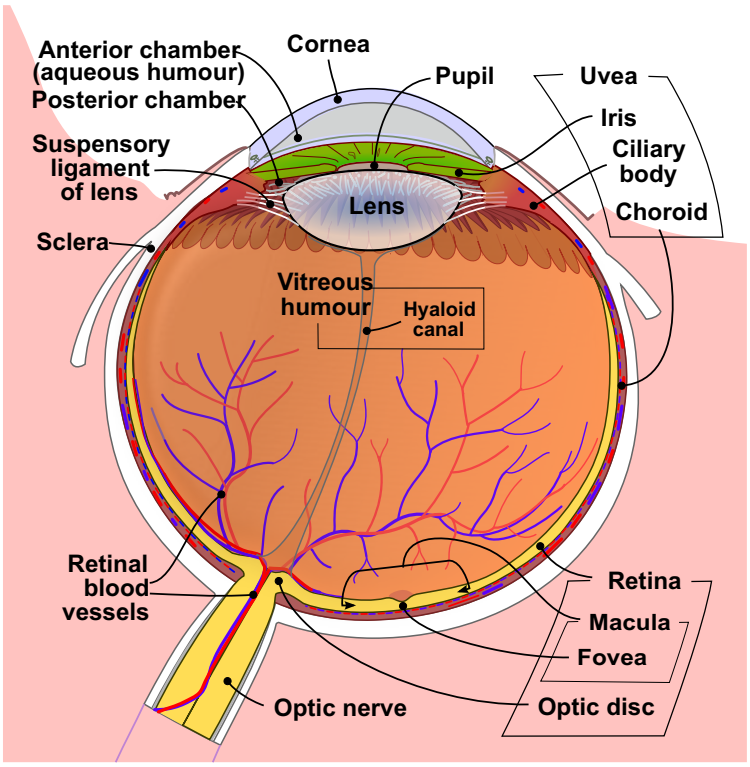

Figure 1.4: Diagram of the human eye showing naming of the different parts. Adapted from [13].

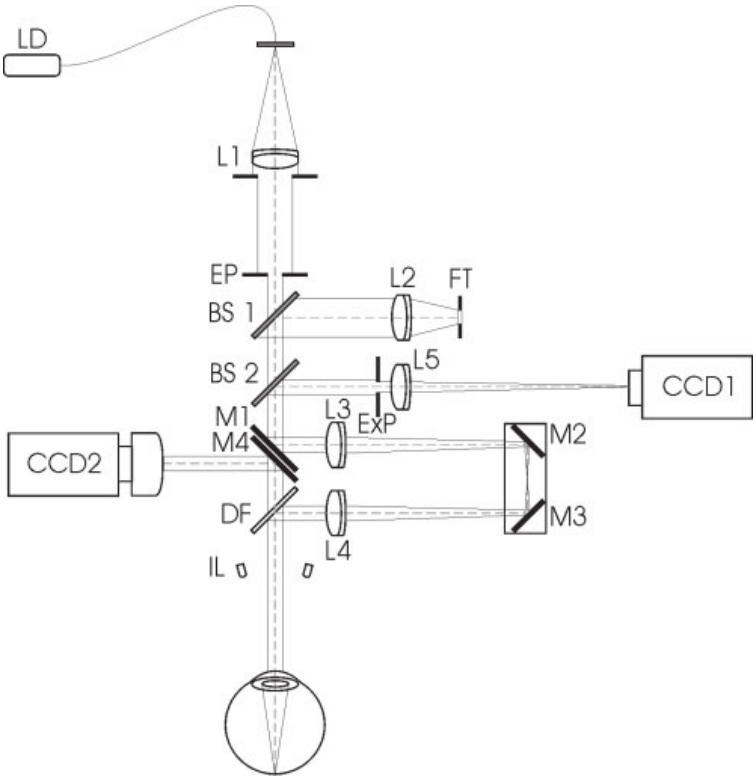

Figure 1.5: Sketch of a double pass (DP) system. LD: laser diode; L1 - L5: lenses; EP, ExP: entrance pupil and exit pupil, BS1 - BS2: beam splitter; M1 - M4: mirrors; DF: dichroic mirror; CCD1, CCD2: ccd cameras, FT: fixation target. Adapted from [14].

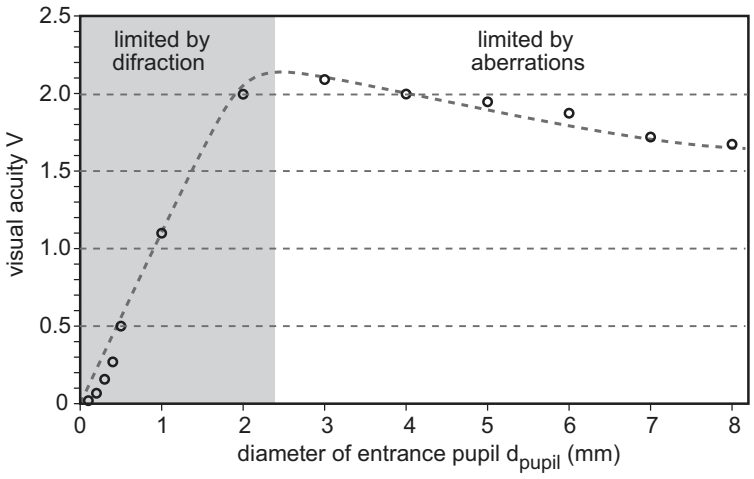

Figure 1.6: Visual acuity as a function of pupil diameter. Visual acuity is a measure of resolution used to determine visual performance. Adapted from [2].

coherent DP retinal image (short exposure) I_i is derived to be

$$\begin{aligned} I_i''(x'', y'') &= |A_i''(x'', y'')|^2 \\ &= m^4 |h_2(mx'', my'') * h_1(-mx'', -my'') R_i(-mx'', -my'')|^2, \end{aligned} \tag{1.1}$$

where x'' and y'' denote the spatial coordinates in the DP imaging plane, A_i'' denotes the amplitude distribution of the DP pass image (aerial image), h_1 is the amplitude-spread function between object plane and retina, $m = |d'/d|$ is the modulus of the magnification (with d and d' being the object and image distance to the eye's lens, respectively), $*$ denotes convolution and R_i the retinal amplitude reflection factor.

If we assume a series of N coherent DP images to have uncorrelated speckle realizations, and the retinal reflection factor $R_i(x'', y'')$ to be a complex function with unit modulus and a random phase, the incoherent (averaged) double pass image is

$$\begin{aligned} I''(x'', y'') &= \frac{1}{N} \sum_{i=1}^{N} I_i''(x'', y'') \\ &\propto |h_2(mx'', my'')|^2 * |h_1(-mx'', -my'')|^2 \\ &= PSF_2(mx'', my'') * PSF_1(-mx'', -my''), \end{aligned} \tag{1.2}$$

where PSF_1 refers to the retinal image of a point test and PSF_2 refers to the image of a point test in the retinal plane. If PSF_1 and PSF_2 are equal, the DP retinal image is related to the single pass PSF, PSF_1, by autoconvolution with a negative sign in the argument of one of the PSF_1, which equals the autocorrelation of the PSF [5].

Often, the radial profile of the double pass PSF is a helpful plot. We obtain it by radially averaging the DP image from its center $(\bar{x}, \bar{y})$. The center can be defined as the centroid of the intensity distribution of the DP image:

$$\bar{x} = \frac{\int dx \int dy\, x\, I''(x, y)}{\int dx \int dy\, I''(x, y)}, \qquad \bar{y} = \frac{\int dx \int dy\, y\, I''(x, y)}{\int dx \int dy\, I''(x, y)}. \tag{1.3}$$

The single pass ocular PSF can not be obtained from alive eyes. However, later in the thesis we use the term "PSF" to refer to the DP image (which is actually the convolution of first and second pass PSFs).

1.1.2 Modulation transfer function

The modulation transfer function (MTF) describes the image contrast C as a function of the spatial frequency. The MTF is an important parameter for measuring imaging quality of optical systems.

The ocular MTF can be calculated from the DP image as

$$\begin{aligned} MTF(u,v) &= |\mathcal{F}(I''(x'',y''))|^{1/2} \\ &= |\mathcal{F}(PSF_2(mx'',my'') * PSF_1(-mx'',-my''))|^{1/2} \\ &= |\mathcal{F}(PSF_2(mx'',my''))\mathcal{F}(PSF_1(-mx'',-my''))|^{1/2} \\ &= |OTF_2(u,v)OTF_1(-u,-v)|^{1/2} \\ &= |OTF_2(u,v)OTF_1^*(u,v)|^{1/2}, \end{aligned} \tag{1.4}$$

where $\mathcal{F}$ means Fourier transformation,

$$OTF(u,v) = MTF(u,v) \cdot \exp\left(i\, PTF(u,v)\right) = \mathcal{F}(PSF(mx'',my'')) \tag{1.5}$$

is the optical transfer function and u, v are coordinates of spatial frequency along two perpendicular directions. $PTF(u,v)$ represents the phase transfer function (PTF).

For DP images obtained with equal entrance and exit pupils, phase information is lost (the PTF is a constant) because the Fourier transform of the DP image $I''(x'',y'')$ (Eq. 1.2), which is a real and even function, is also a real and even function [5] (see also equation 1.4).

If a small entrance pupil (diffraction limited) is used in the first pass and a larger exit pupil in the second pass, phase information is preserved and aberrations in the first pass can be neglected (see Fig. 1.6). Thus, the first pass is only affected by aberrations, whose form is known to be an Airy disc with phase zero. Consequently, the OTF of the eye can be approximated as

$$OTF_{eye} = \frac{OTF_2(u,v)OTF_1^*(u,v)}{OTF_{dl}(u,v)} \approx OTF_2(u,v) \tag{1.6}$$

with the diffraction-limited OTF for the first pass pupil diameter OTF_{dl} However, here we only use the MTF, which is the modulus of the OTF.

We use the one-dimensional MTF, which we obtain by averaging across all angles:

$$MTF(\nu) = \frac{1}{2\pi}\int_0^{2\pi} d\varphi\, MTF(\nu,\varphi) \tag{1.7}$$

with the radial spatial frequency $\nu = \sqrt{u^2+v^2}$. In visual optics, the unit cycles/degree = cyc/deg is usually used for spatial frequencies. It is equal to the number of cycles of a grating that subtends an angle of one degree at the eye.

A DP image and its corresponding PSF profile and MTF profile are shown in Fig. 1.7.

For comparison we present the DP images of a young healthy eye and an extreme case of astigmatism in Fig. 1.8.

1.1.3 Quantifiers of the optical quality of the eye

From the PSF and MTF several measures that quantify the optical quality of the eye can be computed. In the following, we describe the most used ones, although not of special importance for this thesis, which focuses on speckle reduction.

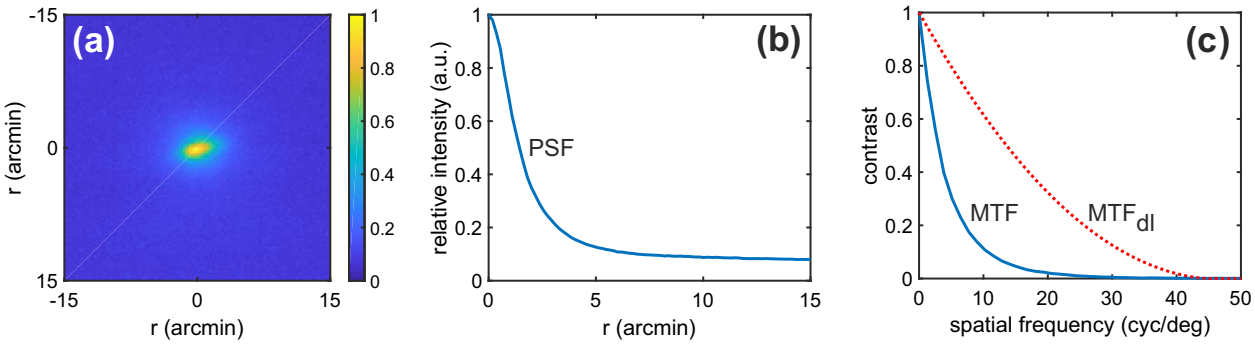

Figure 1.7: (a) Normalized DP image of an eye (circular entrance pupil of 2 mm diameter, wavelength used 780 nm), intensities depicted by color. (1 arcmin = 1°/60) (b) Normalized radial profile of the PSF. (c) Blue line: profile of the MTF (see equation 1.7). Red dashed line: diffraction limited MTF (calculated according to [15]). The optical quantifiers discussed in subsection 1.1.3 obtained from this image are: Strehl ratio = 0.33, MTF cutoff frequency = 24.44 cyc/deg and objective scatter index = 0.066.

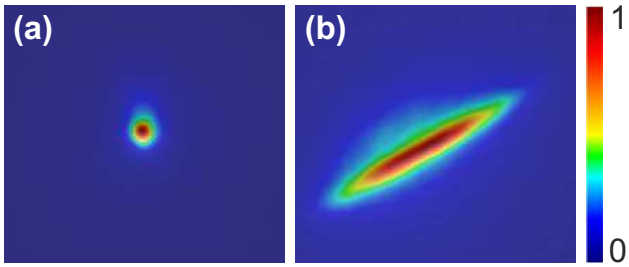

Figure 1.8: Normalized DP images. Both images show an angle from -19.7 arcmin to +19.7 arcmin horizontally and vertically. (a) Young healthy eye. (b) Eye with 4 D of astigmatism (1 D = 1 diopter = 1/m). Taken from [16].

Strehl ratio

The Strehl ratio (SR) is frequently used to quantify the image quality of the PSF. Usually, it is defined as the ratio of the intensity of the PSF in the center of the image and the theoretical maximum intensity of a perfect (diffraction limited, index dl) optical system:

$$SR = \frac{PSF(0,0)}{PSF_{dl}(0,0)} \tag{1.8}$$

It indicates the level of image quality in the presence of aberrations and has a value between 0 and 1, where 1 describes a perfectly unaberrated system. Alternatively, the SR can be calculated in the Fourier domain as the area under the OTF of an eye over the area under the OTF curve of a diffraction limited system:

$$SR = \frac{\int_{-\infty}^{\infty} du \int_{-\infty}^{\infty} dv\, OTF(u,v)}{\int_{-\infty}^{\infty} du \int_{-\infty}^{\infty} dv\, OTF_{dl}(u,v)}. \tag{1.9}$$

In practice, instead of the OTF the MTF is often used since the PTF is not known in many cases [17].

We determine the SR from the radially averaged MTF:

$$SR = \frac{\int_{0}^{\infty} d\nu\, MTF(\nu)}{\int_{0}^{\infty} d\nu\, MTF_{dl}(\nu)}. \tag{1.10}$$

This definition yields slightly different results than the methods described in equations 1.8 and 1.9 [17].

Typical SR values for young (< 30 years) healthy eyes are $SR = 0.27 \pm 0.06$ [18].

MTF cutoff frequency

The cutoff frequency ν_{cutoff} is the frequency where the MTF reaches a value of zero. Object details of higher spatial frequencies have no contrast in the image and can thus not be resolved. There is an upper limit of the cutoff frequency which can only be achieved by a diffraction-limited optical system:

$$\nu_0 = \frac{\pi}{180}\frac{D}{\lambda}\text{cycles/degree} \tag{1.11}$$

for light of wavelength λ and an aperture diameter D. For example, if we have light with a wavelength of 780 nm and an aperture of 2 mm diameter, the theoretical maximum resolvable frequency is $\nu_0 = 44.752$ cycles/degree (see Fig. 1.7(c)).

When determining the cutoff frequency ν_{cutoff} experimentally, we use the frequency where the MTF falls to 0.01 instead of zero for numerical reasons and because noise in the PSF contributes to high spatial frequency components in the MTF [18].

Typical MTF cutoff frequency values for young (< 30 years) healthy eyes are $\nu_{\text{cutoff}} = 44.54 \pm 7.14$ [18].

Objective scatter index

The more scattering occurs in the eye, the more intensity is found in the outer parts of the DP image. Scattering in the eye is specifically quantified by the objective scatter index [19]. It is defined as the ratio of the intensity found in the ring located between 12 and 20 arcmin away from the central peak, I_R, and the intensity of the central peak of the DP image within 1 arcmin, I_0:

$$OSI = a\frac{I_R}{I_0} \tag{1.12}$$

with a scaling factor a. In [19], $a = 0.1$ was chosen to limit OSI values from 0 to 25. We use the same value.

If used for cataract classification, values of $OSI < 1$ are found in healthy eyes, while values $OSI > 7$ correspond to severe cataracts.

1.1.4 Eye safety

When working with lasers and alive eyes, laser safety regulations have to be taken into account. According to the standard IEC 60825-1:2008 [20] on laser product safety, the maximum permissible exposure (MPE) at the corneal surface for laser light of wavelengths $\lambda = 700 - 1050$ nm is

$$\mathrm{MPE} = 18 \cdot t^{0.75} \cdot C_4 \frac{\mathrm{J}}{\mathrm{m}^2}, \tag{1.13}$$

with the parameter $C_4 = 10^{0.002(\lambda - 700)}$ and the time of exposure t. In particular, for a laser source of wavelength $\lambda = 780\,\mathrm{nm}$, $C_4 = 1.45$. For $t = 1\,\mathrm{s}$, Eq. 1.13 gives $\mathrm{MPE} = 26.02\,\mathrm{J/m^2}$. If the laser beam passes a circular entrance pupil of diameter $d = 2\,\mathrm{mm}$ (area $A = \pi d^2/4 = 3.1416 \cdot 10^{-6}\,\mathrm{m}^2$), and we assume it has a flat top beam profile afterwards, the eye can be exposed to an energy of

$$\mathrm{MPE(J)} = 26.02\,\frac{\mathrm{J}}{\mathrm{m}^2} \cdot 10 \cdot 10^{-6}\,\mathrm{m}^2 = 81.738\,\mu\mathrm{J}. \tag{1.14}$$

Or, for a maximum measurement time of 1 s, the eye can be exposed to a power of $\mathrm{MPE(W)} = 81.738\,\mu\mathrm{W}$.

1.1.5 Applications of DP imaging

DP imaging can be used e.g., for planning refractive surgery [21], which is usually done for correction vision disorders like myopia, hyperopia and astigmatism, or degenerative disorders like keratoconus as well as for post-operative checkups. It can also be used to assess intraocular scattering, e.g. for cataract classification [19, 22], as well as for tear film evaluation [23].

A commercial DP device is depicted in Fig. 1.9. It consists of a height-adjustable chin rest for the patient and a housing that contains the DP system and is movable with respect to the patient. The device is connected to a PC in order to calculate the quantifiers of the optical quality (e.g. SR, MTF cutoff frequency and OSI) and display the results.

Figure 1.9: Commercially available DP system (HD Analyzer by Visiometrics [24]).

1.2 Light sources

Laser diodes are a fundamental part of most DP systems. Here, we introduce lasers and afterwards we explain the basics of semiconductor light sources.

1.2.1 Lasers

Fundamental work for the development of the laser was done in the beginning of the 20th century, with the development of theories describing the quantum nature of interactions between light and matter. In 1900, Planck deduced the relationship between energy and frequency of radiation and stated that energy could only be absorbed or emitted in discrete quanta [25]. In 1905, Einstein published his paper on the photoelectric effect [26] and in 1917, he put forward hypotheses about the energy exchange through radiation [27], introducing stimulated emission, an elementary process of a laser, which is an acronym for "light amplification by stimulated emission of radiation". Figure 1.10 shows a diagram of absorption, spontaneous emission and stimulated emission processes. Absorption means that an incident photon is eliminated while matter is excited from a lower to a higher quantum-mechanical energy state. An excited energy state has a particular lifetime, after which it decays and releases a photon with random phase and direction. This process is called emission. The process of stimulated emission also requires an excited energy state, as shown in Fig. 1.10(c), but the transition rate to the lower state is increased beyond that of spontaneous emission by an incident photon. The emitted photon is identical to the incident photon, i.e. it has the same direction, frequency and phase.

The first theoretical description of a laser is attributed to Schawlow and Townes in 1958 [28]. The essential components for any laser are a gain medium, in which stimulated emission takes

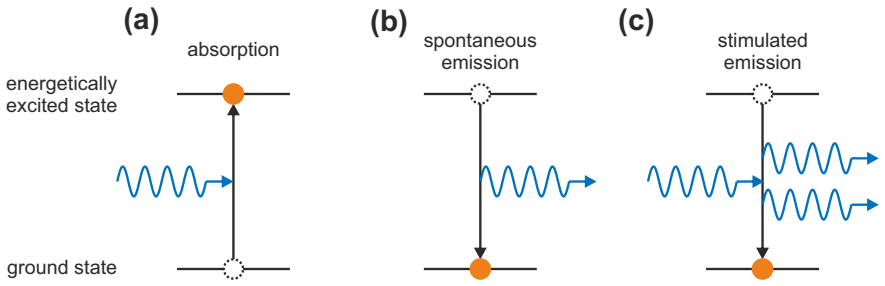

Figure 1.10: Representation of the processes absorption, spontaneous emission and stimulated emission of photons (blue wavy lines) in a two-level energy diagram. The white dashed circle represents the level occupation before the process, the orange filled circle after the process.

place, a pumping mechanism to achieve population inversion in the gain medium, and a cavity that confines photons to the gain medium. The first working laser was presented in 1960 by Maiman and consisted of a ruby crystal acting as active medium, with two parallel faces that were coated with silver, serving as the resonator, while pumping was achieved through a high-power flash lamp [29, 30].

Figure 1.11 shows the power curve of a laser, i.e. its light output as a function of the pump power employed. At low pump powers, spontaneous emission dominates the output. Increasing the pump power leads to a small increase in the output. When the pump power is further increased, the gain grows and reaches a point where it is equal to the losses. This point is the lasing threshold (marked by the red line). Above this pump power, stimulated emission dominates, and a regime of steeper linear dependence of the output power on the pump power begins. The regime of stimulated emission does not start abruptly, thus there is not just one definition for the threshold. We define it as the maximum of the second derivative of the power curve.

In contrast to other light sources, lasers emit light coherently, i.e. the light has a constant phase difference over time and space. Due to their spatial coherence, laser beams can stay collimated over large distances and be focused to tight spots, while their temporal coherence can be used to obtain a narrow optical spectrum or ultrashort pulses with a broad optical spectrum.

Various different media can be used as gain media, which has given rise to solid state, gas, fiber, and semiconductor lasers. Semiconductor lasers, in particular, are popular because they are efficient, inexpensive and cover a wide range of wavelengths.

There are also many ways of realizing laser cavities. Some geometries can be beneficial for increasing the output power before the gain medium saturates or for the beam quality. A Fabry-Pérot cavity is formed by two mirrors facing each other, one of them slightly light-transmissive. Mirrors can be arranged concentrically, or the cavity can be rectangular or triangular. Specially designed D-shaped cavities feature chaotic ray dynamics [31]. Nanolasers can be made within

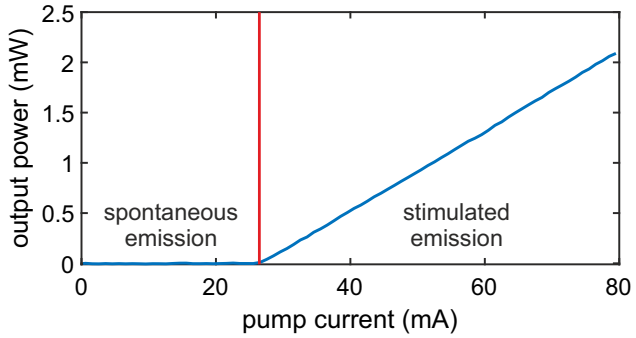

Figure 1.11: Power curve of a laser diode (Thorlabs HL6750MG) in the linear regime. Pumping is achieved by injecting a current, thus the x-axis reads current instead of power. The red line approximately marks the pump current above which lasing is possible, the lasing threshold. At higher pump currents than the ones shown here, the linear behavior is not given anymore.

photonic crystals. Optical fibers can also serve as cavities.

The high possible intensity output of lasers, their beam directionality and focusability, their monochromaticity and their capability to create ultrashort pulses make lasers attractive for many applications as well as fundamental research. Nowadays, lasers are widely used, e.g. for medical treatments, many of them in the field of ophthalmology; for laser cutting and welding, in information technology for reading and writing on optical disk drives, for lithography as well as fiber-optic telecommunication; in interferometry and for specific imaging applications like confocal laser scanning microscopy or in laser projectors.

Coherence

As mentioned before, most lasers emit light coherently. Coherence in optics refers to the correlation of electromagnetic waves, i.e. the phase-relation of the wavefronts. It is important to distinguish between temporal coherence and spatial coherence. When we talk about temporal coherence, we refer to the possibility of a light beam to interfere with a time-delayed version of itself, like it happens in a Michelson interferometer. Temporal coherence is related to the spectral width of a source. Spatial coherence, on the other hand, refers to whether a spatially shifted (but not time-delayed) light beam can interfere with the non-shifted beam. Young's double slit experiment is based on spatial coherence (but also temporal coherence).

Temporal coherence can be quantified by the self-coherence function, i.e. the autocorrelation function of the analytic signal $u(t)$ of the light emitted by a source [32]:

$$\Gamma(P_1,\tau) = \langle u(P_1,t+\tau)u^*(P_1,t)\rangle = \lim_{T\to\infty}\frac{1}{2T}\int_{-T}^{T} dt\, u(P_1,t+\tau)u^*(P_1,t), \tag{1.15}$$

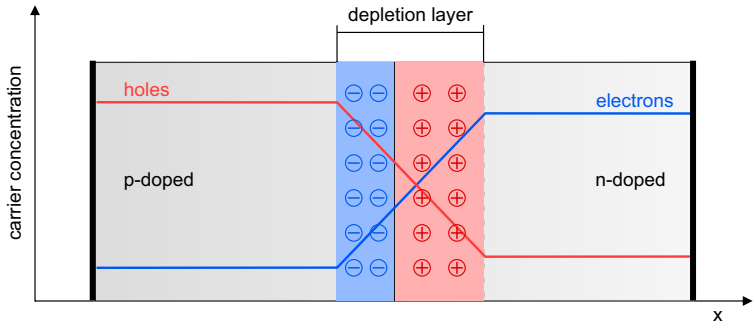

Figure 1.12: Carrier concentration of a p-n junction in equilibrium and resulting depletion zone.

or by the normalized version, called complex degree of coherence:

$$\gamma(P_1, \tau) = \frac{\Gamma(P_1, \tau)}{\Gamma(P_1, 0)}, \tag{1.16}$$

with $\gamma(0) = 1$, $|\gamma(\tau)| \leq 1$.
The coherence time is defined as [32, 33]

$$\tau_c = \int_{-\infty}^{\infty} d\tau |\gamma(\tau)|^2 \tag{1.17}$$

and in [32], a reciprocal relation with the bandwidth is derived:

$$\tau_c \propto \frac{1}{\Delta\nu} \propto \frac{1}{\Delta\lambda}. \tag{1.18}$$

1.2.2 Semiconductor light sources

Laser diodes, light emitting diodes and superluminescent light emitting diodes are all electrically pumped semiconductor diodes. They are based on p-n junctions, i.e. the border in a crystal between negatively (n) and positively (p) doped regions. Next to this border, some of the additional electrons diffuse from the n-doped region through the junction and recombine with holes in the p-region, forming a barrier between the two regions called depletion layer (as shown in Fig. 1.12).

If a voltage is applied to a semiconductor diode in forward direction (positive voltage to the p-side), electrons migrate from the n-doped part to the p-n junction and cross to the p-doped part, where they skip to the energetically favorable valence band as shown in Fig. 1.13. In direct band gap semiconductors, this process of recombination (of an electron from the conduction band and a hole from the valence band), energy is released in form of photons.

Light emitting diodes

The light of light emitting diodes (LEDs) is based on spontaneous emission and thus not coherent. Since spontaneous emission creates isotropic light, LED light is not collimated and its opening

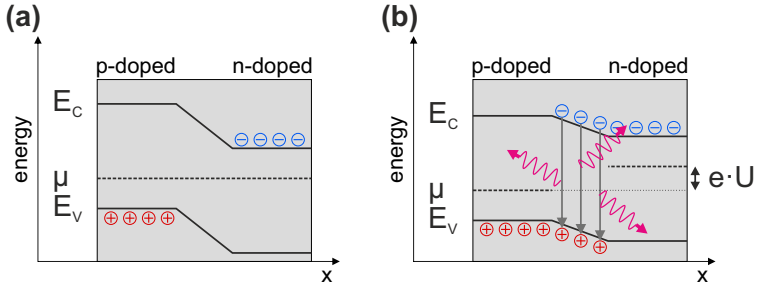

Figure 1.13: Energy diagram of a p-n junction (a) in equilibrium and (b) with a forward voltage applied. E_V: valence band energy, E_C: conduction band energy, μ: chemical potential, U: applied voltage.

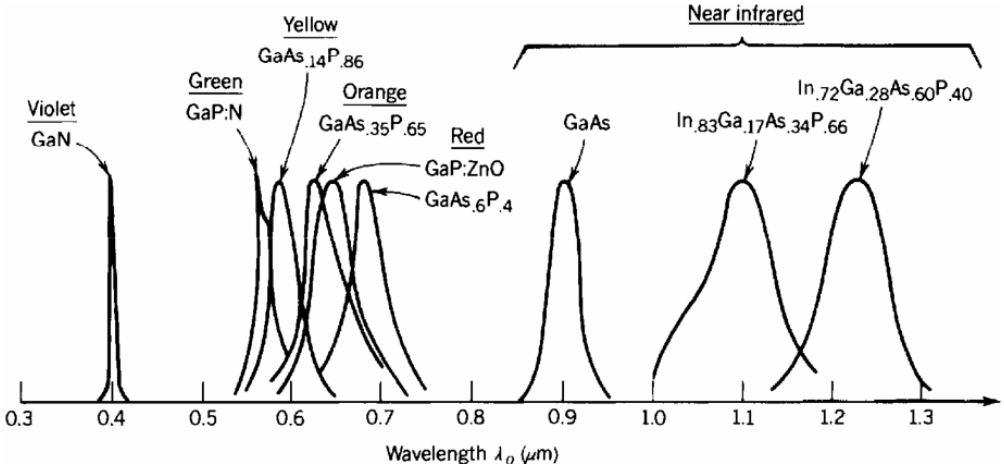

Figure 1.14: Spectra for various semiconductor material compositions with different bandgaps. Adapted from [33].

angle has to be regulated by reflectors. The central emission wavelength of LEDs is determined by the energy of the electronic transition of the semiconductor junction. Thus it is relatively narrow-banded compared to thermal radiation sources. The linewidth of LED spectra depends on λ according to

$$\Delta\lambda \approx 1.45\lambda_p^2 k_\mathrm{B}T, \tag{1.19}$$

where $k_\mathrm{B}T$ is expressed in eV, λ is expressed in µm, $\lambda_p = c/\nu_p$ and $\nu_p = (E_g + k_\mathrm{B}T/2)/h$ is the frequency at which the spectral density achieves its peak value (E_g: band gap energy, h: Planck constant) [33]. This dependence is apparent in Fig. 1.14.

The output optical power of a typical LED is plotted in Fig. 1.15(a). Since an LED is based on spontaneous emission, the optical power emitted is proportional to the injected current and there is no emission threshold. For high injection currents proportionality fails due to thermal effects and gain saturation [33].

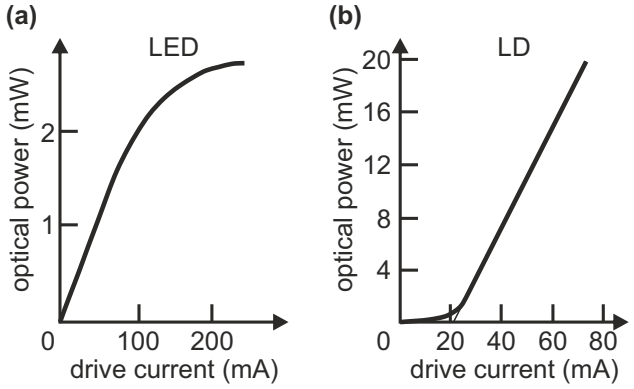

Figure 1.15: Output power as a function of the drive current for (a) an LED and (b) an InGaAsP heterostructure LD. After [33].

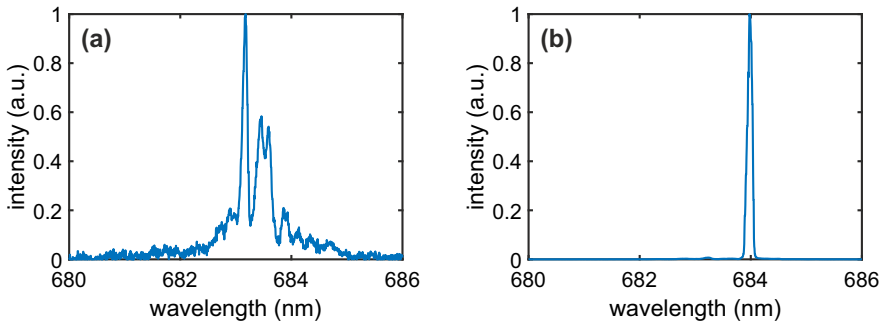

Figure 1.16: Normalized optical spectra of an LD (Thorlabs HL6750MG). (a) $J_\mathrm{p} = 27.2\,\mathrm{mA}$, just above and (b) $J_\mathrm{p} = 45.0\,\mathrm{mA}$, far above the threshold current $J_{\mathrm{p,\,thr}} \approx 26.7\,\mathrm{mA}$.

Laser diodes

Pumping of laser diodes is achieved by distributing charge carriers to the active region by applying a pump current.

The cavity of a semiconductor laser can be realized as Fabry-Pérot cavity, which consists of two parallel cleaved end facets of the semiconductor crystal. With a typical reflective index of the semiconductor material of $n \approx 3$, the reflectivity of a cleaved facet is only around 25 %. One of the facets can be coated with a total-reflection coating to increase output power. Another possible cavity is the distributed Bragg reflector (DBR) cavity, in which one or two Bragg reflectors such as gratings are used. Since the frequency selectivity of Bragg reflectors can be very narrow, they can be used for single longitudinal mode laser operation. But even with Fabry-Pérot cavities, quasi single mode emission can be achieved, depending on cavity design, temperature and pump current. Typical spectra of an LD for pump currents just above threshold (multimode) and far above threshold (quasi singlemode) are shown in Fig. 1.16.

The resonator length L of semiconductor lasers is usually on the order of hundreds of micrometers

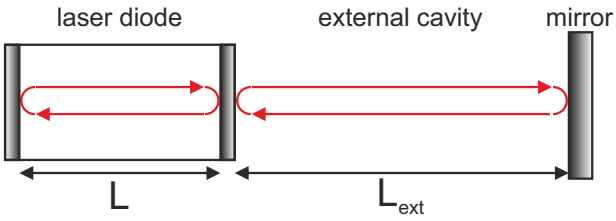

Figure 1.17: Achieving optical feedback by mirror in front of the LD cavity. After [35].

to millimeters. The free spectral range (longitudinal mode spacing) is $\Delta\nu_L = c/(2n_gL)$, where c is the speed of light, n_g is the group refractive index.

Aside from the edge emitting lasers used in this thesis (which have output powers between a few milliwatts and half a watt), there are vertical-cavity surface-emitting lasers (VCSELs), in which light travels in the direction perpendicular to the active region. VCSELs can reach output powers of a few milliwatts with high beam quality.

Laser diode properties can be tuned by the choice of semiconducting materials (e.g. III-V-compound semiconductor for short emission wavelengths), doping, heterostructures of different materials (e.g. to obtain multiple quantum wells for increased gain).

Typical output powers of a InGaAsP heterostructure LD ($\lambda = 1.3\,\mu m$) are plotted in Fig. 1.15(b). Only the linear regime is shown; saturation due thermal and nonlinear effects occurs at higher pump currents.

Superluminescent diodes

Superluminescent diodes (SLEDs) are based on amplified spontaneous emission, i.e. light produced by spontaneous emission is optically amplified by stimulated emission. Like laser diodes, they possess a gain medium that is electrically pumped, but lasing is inhibited by the absence of a resonant cavity. This is achieved by suppressing any optical feedback, e.g. by tilting the facets relative to the waveguide and furthermore by the use of anti-reflection coatings. An SLED's optical spectrum is determined by the bandwidth of the gain medium and can typically reach a few tens to one hundred nanometers (at infrared wavelengths), similar as LEDs. SLED light has low temporal coherence, but in contrast to LED light, it can have high spatial coherence, meaning that it has high directionality and can be focused to a tight spot.

1.2.3 Optical feedback

Optical feedback means that part of the emitted light is directed back into the cavity of an LD. This is typically achieved by putting a mirror in front of the cavity as shown schematically in Fig. 1.17, also known as external cavity [34]. Light can be coupled out of the external cavity by employing a partially reflective end mirror or by using a beam splitter in the external cavity.

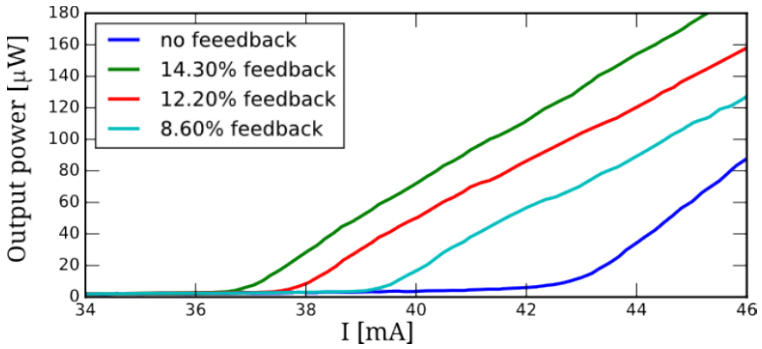

Figure 1.18: Power curves of an LD (Hitachi HL6501MG) for different amounts of optical feedback. Adapted from [39].

The three main parameters define optical feedback: the length of the external cavity L_{ext} (which results in a delay time of $\tau = \frac{2L_{\text{ext}}}{c}$ with c being the speed of light), the strength of the feedback and the phase of the reinjected light. In this thesis we do not consider effects of cavity length and phase. Optical feedback induces a rich dynamical behavior [35–38].

As a consequence of optical feedback, the threshold current decreases as compared to the case without optical feedback. The threshold reduction

$$\eta = \frac{J_{\text{p, thr}} - J_{\text{p, thr}}^{\text{FB}}}{J_{\text{p, thr}}} \tag{1.20}$$

can be used to quantify the feedback strength. $J_{\text{p, thr}}$ and $J_{\text{p, thr}}^{\text{FB}}$ represent the threshold currents without/with feedback, respectively. Figure 1.18 shows several LD power curves with/without optical feedback and the corresponding calculated threshold reductions η in percent. If the distance $2L_{\text{ext}}$ which the light travels in the external cavity is longer than the coherence length of the light, or if the reinjected light has orthogonal polarization with reference to the light in the LD, the feedback is incoherent and the threshold current will not be reduced compared to the case without feedback.

Five regimes of feedback were identified in [40], in function of feedback power ratio and distance to reflection (Fig. 1.19). **Regime I:** For the lowest amount of feedback, depending on its phase, a narrowing or broadening of the emission line is observed. **Regime II:** Depending on the distance to the external reflector and the strength of the feedback, the broadening from Regime I changes to a splitting of the emission line due to rapid mode hopping. **Regime III:** Increasing the feedback level, a distance-independent regime is reached in which mode hopping is suppressed and there's a single narrow emission line. **Regime IV:** Further increasing the amount of feedback, there's another distance-independent regime in which satellite modes appear that are separated from the main mode by the relaxation oscillation frequency.[1] This regime is also termed "coherence collapse",

[1] Relaxation oscillations are oscillations in the output power that occur upon changing the pump current of LDs.

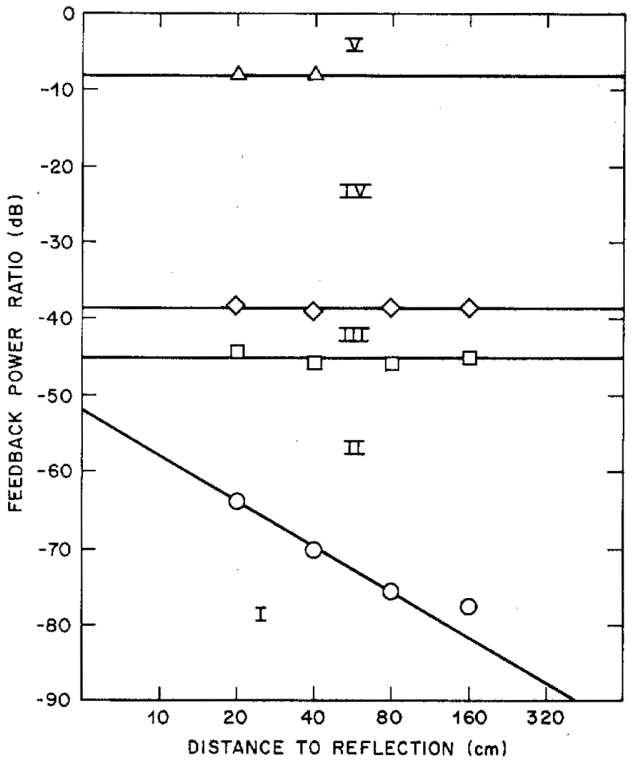

Figure 1.19: Regimes of optical feedback. Adapted from [40].

because the coherence length is drastically reduced and the laser linewidth increases up to as much as 50 GHz. **Regime V:** At highest levels of feedback, there's stable narrow-banded single mode emission. The external cavity becomes the main cavity of the laser, and inside of it the semiconductor acts as a short active region.

Whenever using optical feedback in this thesis, we are interested in regime IV, where coherence collapse takes place. For that reason we use moderate feedback and a long external cavity ($L_{\text{ext}} \approx 0.5\,\text{m}$), i.e. $\tau \approx 5\,\text{ns}$.

Optical feedback into SLEDs has to be avoided because they are very susceptible to it. Even small amounts of optical feedback strongly deteriorate their performance and can cause fatal device failure due to catastrophic optical damage of the SLED facet [41].

1.3 Speckle

Because DP instruments use laser light, the recorded images show some degree of speckle, an optical phenomenon of coherent waves interfering with each other. In this section we discuss the physical mechanism responsible for speckle, the measures used to quantify it, and the methods that have been proposed to mitigate or suppress speckle. We also mention some optical techniques that

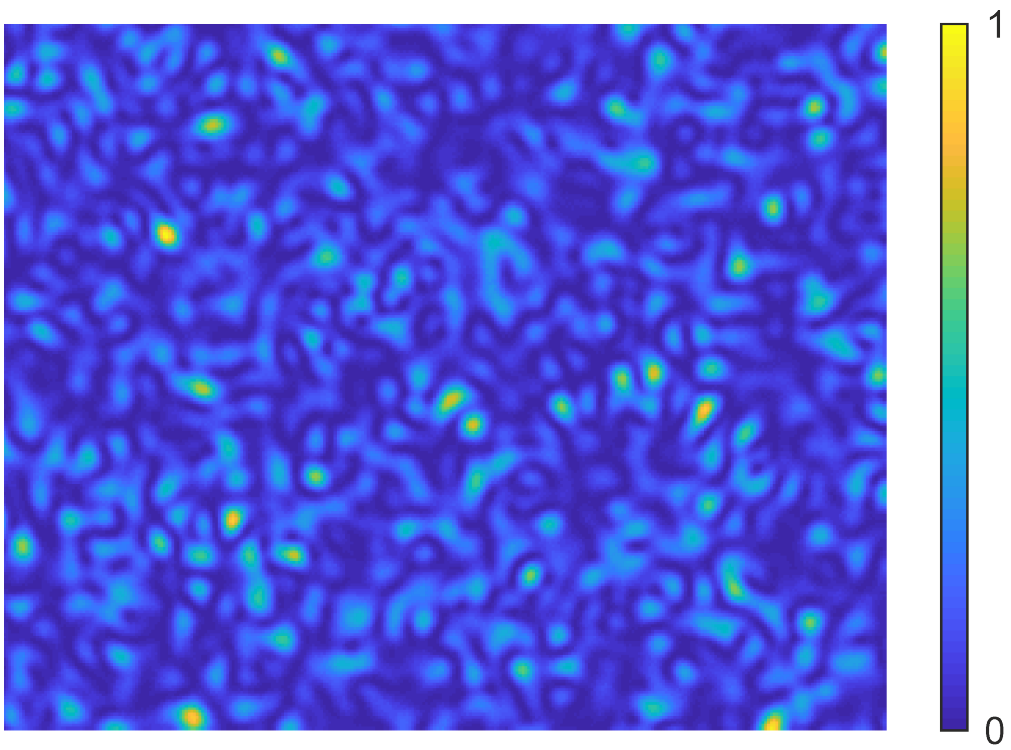

Figure 1.20: Example image of a speckle pattern. The intensity levels of the black and white photograph are colored according to the color bar for better visibility. Here, speckle originates from laser light transmitted through a ground glass and is directly imaged by a camera.

exploit the information contained in speckle patterns to infer properties of the object or of the light generating the pattern.

In practice, it appears when laser light with high spatial and temporal coherence is transmitted through or reflected by an object that is rough on the scale of the wavelength of the light, such that the scattered light interferes, and forms an apparently random distribution of dark and bright spots known as a speckle pattern [42, 43]. An exemplary speckle pattern is shown in Fig. 1.20.

Speckle can be described as the result of a "random walk" [43], i.e. the summation of many complex components (components having both an amplitude and a phase) with random directions (phases) and known or random lengths (amplitudes) in the complex plane. Depending on the phases of the single components, they add up (or interfere) constructively or destructively to a total amplitude as depicted in Fig. 1.21(a) and (b), respectively.

The random walk process can mathematically be described as a random phasor sum:

$$\mathbf{A} = Ae^{i\theta} = \frac{1}{\sqrt{N}} \sum_{n=1}^{N} \mathbf{a}_n = \frac{1}{\sqrt{N}} \sum_{n=1}^{N} a_n e^{i\phi_n}, \tag{1.21}$$

where N is the number of phasor components in the random walk, $\mathbf{A}$ the resultant vector, A its

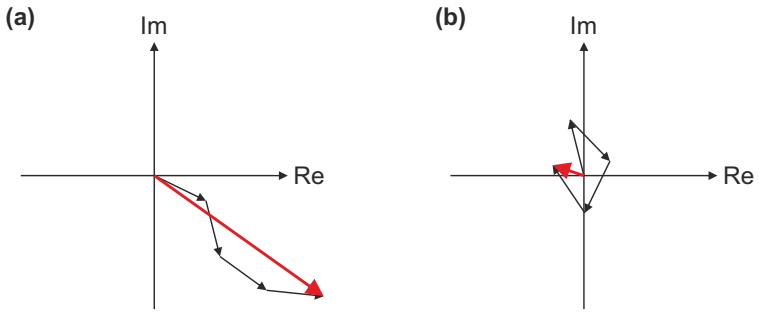

Figure 1.21: Random walks. The thick red arrows represent the sum of the complex components. (a) Constructive summation. (b) Destructive summation.

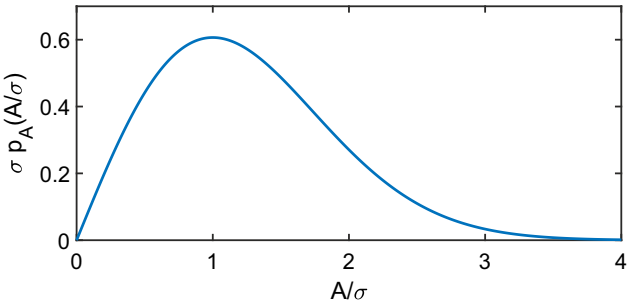

Figure 1.22: Rayleigh probability density function.

length and θ its phase; $\mathbf{a}_n$ is the nth component phasor, a_n its length and ϕ_n its phase. $1/\sqrt{N}$ is a scaling factor preserving finite second moments of the sum even for $N \to \infty$ [44].

The square of the resultant of the random walk represents the intensity:

$$I = A^2. \tag{1.22}$$

Assuming **(i)** that for $m \neq n$, the phases ϕ_n and lengths a_n are statistically independent from ϕ_n and a_n, **(ii)** that for any n, ϕ_n and a_n are statistically independent, and **(iii)** that all phases are equally likely (ϕ_n are uniformly distributed on $(-\pi, \pi)$), and employing the central limit theorem, we obtain a joint probability density function (PDF) of the real and imaginary parts of the resultant phasor $\mathbf{A}$ that is asymptotically Gaussian for $N \to \infty$. After a variable transformation to A and θ (see [44] for details) it follows that A (length) and θ (phase angle) are statistically independent and that the statistics of the length follows a Rayleigh density function:

$$p_A(A) = \frac{A}{\sigma^2} \exp\left\{-\frac{A^2}{2\sigma^2}\right\} \tag{1.23}$$

for $A > 0$, as illustrated in Fig. 1.22.

For a monotonic transformation $v = f(u)$ of a random variable u of a PDF $p_U(u)$, we can find

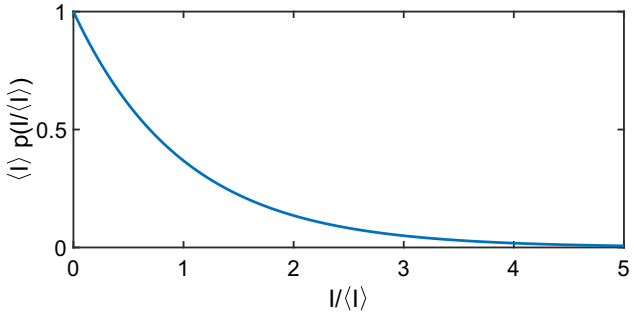

Figure 1.23: Negative exponential PDF.

$p_V(v)$ to be [32]:

$$p_V(v) = p_U(f^{-1}(v)) \left| \frac{du}{dv} \right|. \tag{1.24}$$

Thus, identifying I in Eq. 1.22 with v and A with u, we obtain for the PDF of the intensity:

$$p_I(I) = p_A(\sqrt{I}) \left| \frac{dA}{dI} \right| = \frac{1}{2\sqrt{I}} p_A(\sqrt{I}). \tag{1.25}$$

If there is a large number N of random phasors with a uniform phase distribution on $(-\pi, \pi)$, i.e. $p_A(A)$ is really Rayleigh distributed as in Eq. 1.23, we obtain from Eq. 1.25

$$p_I(I) = \frac{1}{2\sqrt{I}} \cdot \frac{\sqrt{I}}{\sigma^2} \exp\left\{-\frac{I}{2\sigma^2}\right\} = \frac{1}{2\sigma^2} \exp\left\{-\frac{I}{2\sigma^2}\right\}, \tag{1.26}$$

for $I > 0$. With the moments of this distribution being $\bar{I^q} = (2\sigma^2)^q q!$ (found by direct integration [44]), we find

$$p_I(I) = 1/(\langle I \rangle) \exp(-I/\langle I \rangle), \tag{1.27}$$

i.e. a negative exponential probability distribution of the intensity as shown in Fig. 1.23. Speckle patterns with this intensity distribution are called *fully developed*. The variance and standard deviation for this distribution are given by $\sigma_I^2 = \bar{I}^2$ and $\sigma_I = \bar{I}$, respectively. In general, the intensity PDF will be different for non-uniformly distributed phases of the phasors.

Speckle is usually undesired in imaging because it obfuscates structures and generally reduces the resolution. Due to the coherent laser light often used in DP imaging, and the relative roughness of the human retina on the scale of the wavelength of the light, a speckle pattern is formed, which degrades the DP image (see chapter 2). Figure 1.24 shows a DP image superimposed by speckle. Speckle can make DP images uninterpretable because it alters the parameters characterizing the optical properties of the eye that can be determined from the image. For this reason, we are interested in reducing speckle.

However, speckle reduction is not always desired. Some applications use speckle to their advantage, e.g. for laser speckle contrast imaging in blood flow analysis [45], for recognizing scatterers [46], for realizing compact [47, 48] and high-precision [49, 50] spectrometers, for reconstructing

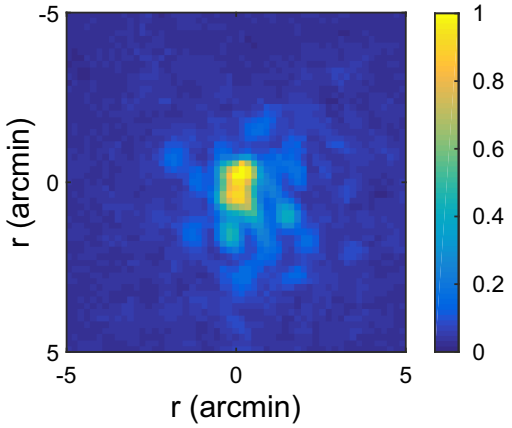

Figure 1.24: DP image showing speckle. Intensity levels are colored for clarity.

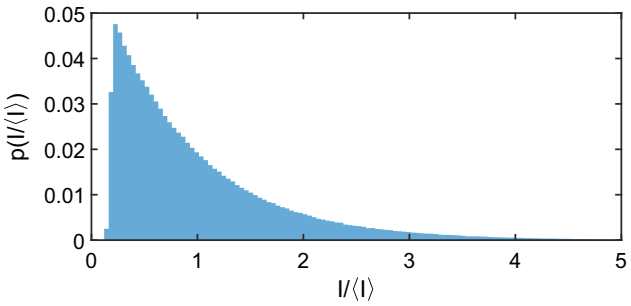

Figure 1.25: Intensity histogram of the speckle pattern shown in Fig. 1.20.

the object from which speckle emerges [51], for imaging through scattering media [52–54] or around corners [55, 56].

1.3.1 Quantification of speckle

To quantify the amount of speckle, the speckle contrast C is widely used. It is defined as the standard deviation of the pattern, σ_I, divided by its mean intensity $\langle I \rangle$:

$$C = \sigma_I / \langle I \rangle \tag{1.28}$$

For fully developed speckle, $C = 1$. The speckle pattern shown in Fig. 1.20 is not fully developed. Its intensity histogram is shown in Fig. 1.25 and its speckle contrast is $C = 0.83$. The histogram shows a close to negative-exponential PDF, but it does not start at zero, meaning there are no black pixels in the speckle image.

Speckle contrast has been used as a quantifier for speckle in full-field imaging, laser projection, microscopy, etc. [44, 57–59].

1.3.2 Speckle reduction techniques

We can reduce the amount of speckle by adding in an intensity basis a number N of uncorrelated speckle patterns, generated by time, space, wavelength or polarization diversity [44]. If the patterns have equal mean intensities, the speckle contrast reduces according to

$$C = \frac{1}{\sqrt{N}} \tag{1.29}$$

If we add, for example, two fully developed speckle patterns (i.e. each of them has $C = 1$) of the same mean intensity, but with orthogonal light polarizations, the speckle contrast of the sum pattern is reduced to $C = 1/\sqrt{2} \approx 0.71$.

In general, speckle is reduced by using spatially and/or temporally partially incoherent illumination [42].

Many speckle reduction or removal techniques have been employed in microscopy, in laser projection, and in other systems that use coherent light sources. For example, a moving diffuser introduced in the beam path randomly modulates the phase, reducing spatial coherence and thus the amount of speckle formed from this light [42]. A typical design consists of a rotating diffuser [60]. In [61], speckle reduction in microscopy is achieved by an LD with optical feedback, which induces a multimode optical spectrum that changes over time. Speckle can also be reduced through illumination from different angles, with different polarizations, or with various wavelengths [44]. Other approaches for speckle reduction consist of employing screens made of microlenses [59], utilizing the intermodal dispersion in long enough optical fibers [62–64] or shaking of multimode fibers.

Speckle reduction in DP imaging

In DP imaging of alive eyes, most speckle can be removed by averaging over many independent short-exposure images (32 in the case of [65]). Other methods have been used, like rotating diffusers [66], acoustic modulation of laser beams [67], periodic variation of the vergence of a lens in the beam [68], and broad-band sources like an SLDs [69, 70]. [71] calculates the required spectral width $\Delta\lambda$ of a source for reducing speckle by producing uncorrelated speckle patterns from retinal reflection. Assuming retinal height fluctuations of $\sigma_z = 1.88\,\mu\text{m}$ (from simulations of scattering from photoreceptors [72]) and a central wavelength of $\lambda_0 = 801\,\text{nm}$, the author obtains

$$\Delta\lambda \approx \frac{\lambda_0^2}{2\sigma_z} \approx 170\,\text{nm}, \tag{1.30}$$

following an equation from [44].

A mechanical method for speckle reduction (that is also used in the commercial system by Visiometrics) uses a vibrating mirror in the beam path of the DP system [69] (in Fig. 1.5, the dichroic mirror DF could act as a vibrating mirror) with a vibration period much shorter than the image exposure time $T = 1/\nu << t_{\text{exp}}$. Typical values are $\nu \approx 100\,\text{Hz} \rightarrow T = 0.01\,\text{s}$ and

$t_{\text{exp}} \approx 250\,\text{ms}$. The vibrating mirror changes the direction of the beam that enters the eye by a small amount, arriving at slightly different positions of the retina, so that different speckle realizations are added during exposure. Since the image is recorded after the second pass, the light passes the vibrating mirror a second time after exiting the eye, so that the light does not move on the imaging plane of the camera.

1.4 Goal of this thesis

This work is motivated by the problem of speckle in DP ocular imaging [4]. Our goal is to find an all-optical and inexpensive solution to reduce speckle in DP images based on semiconductor light source. The advantage in comparison with the vibrating mirror speckle reduction technique would be the absence of mechanically moving parts. The vibrating mirror method not only reduces speckle but it also affects the measured PSF in such a way that measuring dynamics of the PSF, like accommodation fluctuations, or temporal tear film quality analysis are impeded. We furthermore expect to avoid this limitation by using a speckle reduction technique based on the properties of the light employed.

In chapter 2, we present a comparison of a laser diode, a light emitting diode and a superluminescent diode in terms of speckle formation in DP imaging.

As explained before, a possible way to reduce speckle is using broadband illumination, which corresponds to reduced temporal coherence of the light and which can be obtained by inducing optical feedback [61] or by current modulation [35]. In chapter 3, we explore the corresponding effect on speckle formation.

In chapter 4 we investigate the speckle formation of light from a laser diode driven under its threshold current.

Chapter 5 concludes this thesis and presents possible directions of continuing research.

2 Comparison of semiconductor light sources in terms of speckle formation in double pass imaging

The DP technique quantifies the optical quality of the eye by measuring its PSF. The low reflectivity of the retina (2 % to 3 %) requires the use of a high-intensity, point-like illumination source, and thus in DP systems usually laser diodes (LDs) are used. However, LD light produces speckle, and a low-cost solution to reduce speckle is to include a vibrating mirror in the beam path. In this chapter, we use three different semiconductor light sources to perform a comparative study regarding speckle formation in DP imaging of a model eye. With the goal of finding an all-optical solution for speckle reduction, we perform DP measurements using an LD, a light emitting diode (LED), and a superluminescent diode (SLED). Additionally, we compare the results with the speckle reduction that is obtained when a vibrating mirror is used.

Results of this chapter have been published in [73].

2.1 Introduction

In DP systems, mainly due to longitudinal chromatic aberrations of the eye, white-light illumination sources lead to an underestimation of the MTF [74]. Therefore, alternative speckle-reduction solutions have been proposed in the literature, like acoustic modulation of laser beams [67], superluminescent diodes [70], periodic variation of the vergence of a lens in the beam [68], and rotating diffusers [66]. A low-cost solution is the use of a vibrating mirror in the optical path of the DP system as explained in subsection 1.3.2. In this method, the final DP image is the average over many images superimposed by different speckle patterns. However, this method has the disadvantage of moving parts which increase the complexity of the system and make it prone to malfunction because mechanical vibrations can, over time, misalign the optical components of the system. A second disadvantage is the long time needed to perform the measurements, which limits the applicability of the DP technique for real-time dynamic tests, which are needed, for example, for the clinical evaluation of tear film quality and the diagnosis of dry eye syndrome [23].

For this reason in this chapter we present a comparative study of the amount of speckle produced by different semiconductor light sources. In particular, we quantify speckle in DP images of a model

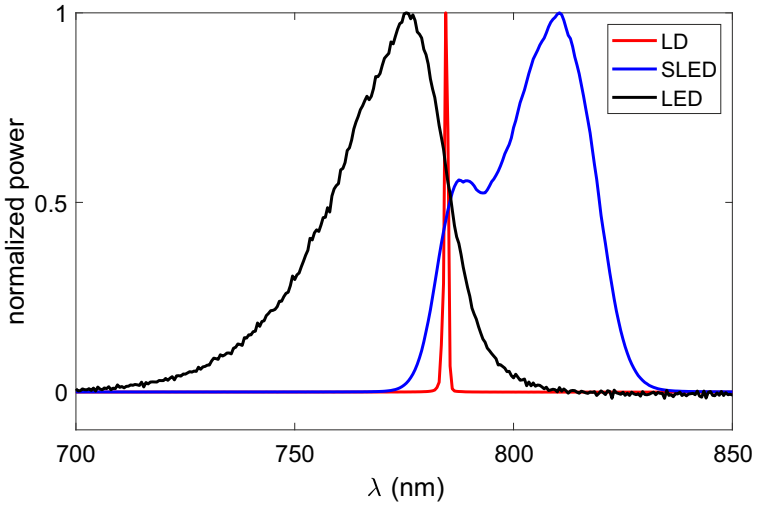

Figure 2.1: Normalized spectra of the light sources used.

eye acquired with an LD, an LED, and an SLED, and compare this to the speckle reduction achieved with a vibrating mirror and each of the mentioned sources.

2.2 Experimental setup

The experimental setup is depicted in Fig. 2.2. By using two 50 % beam splitters, BS1 and BS2, the three light sources used (single-mode LD Monocrom 7850 MC with output power ∼5 mW; Superlum SLED SLD 371 with ∼6 mW, and Thorlabs LED M780F2 with ∼1.15 mW) are fiber-coupled into the optical setup by three collimators (C1 - C3) such that DP images can be compared without the need of realignment after changing the light source. As in clinical instruments, the optical power and wavelengths are chosen to meet the limitations of patient comfort, and therefore, the three light sources emit in the near-infrared. Their optical spectra (measured with an Instrument Systems Spectro 320 spectrometer), are depicted in Fig. 2.1. To couple light from the LED into the system, we used a 25 µm diameter fiber as a trade-off between good collimation and intensity transmitted.

The collimated beam from the light source being used is guided to a model eye or to a real eye (eye), by a hot mirror (hM, with a motor attached which can be used to make it vibrate in order to vary the direction of the reflected beam by a small amount), a Badal system (consisting of two lenses (L1, L2, $f = 150$ mm each) and two mirrors, M1 and M2, mounted on a movable stage for correction of spherical refractive errors of the eye), and a dichroic mirror (dM, cutoff wavelength of 900 nm). The first pass of the light is indicated by red continuous lines. The model eye consists of a 50 mm lens and a black cardboard that mimics the retina (retinal plane and conjugated planes marked in purple). The eye camera EC (IDS UI-1240LE-M) was used to check the position of the

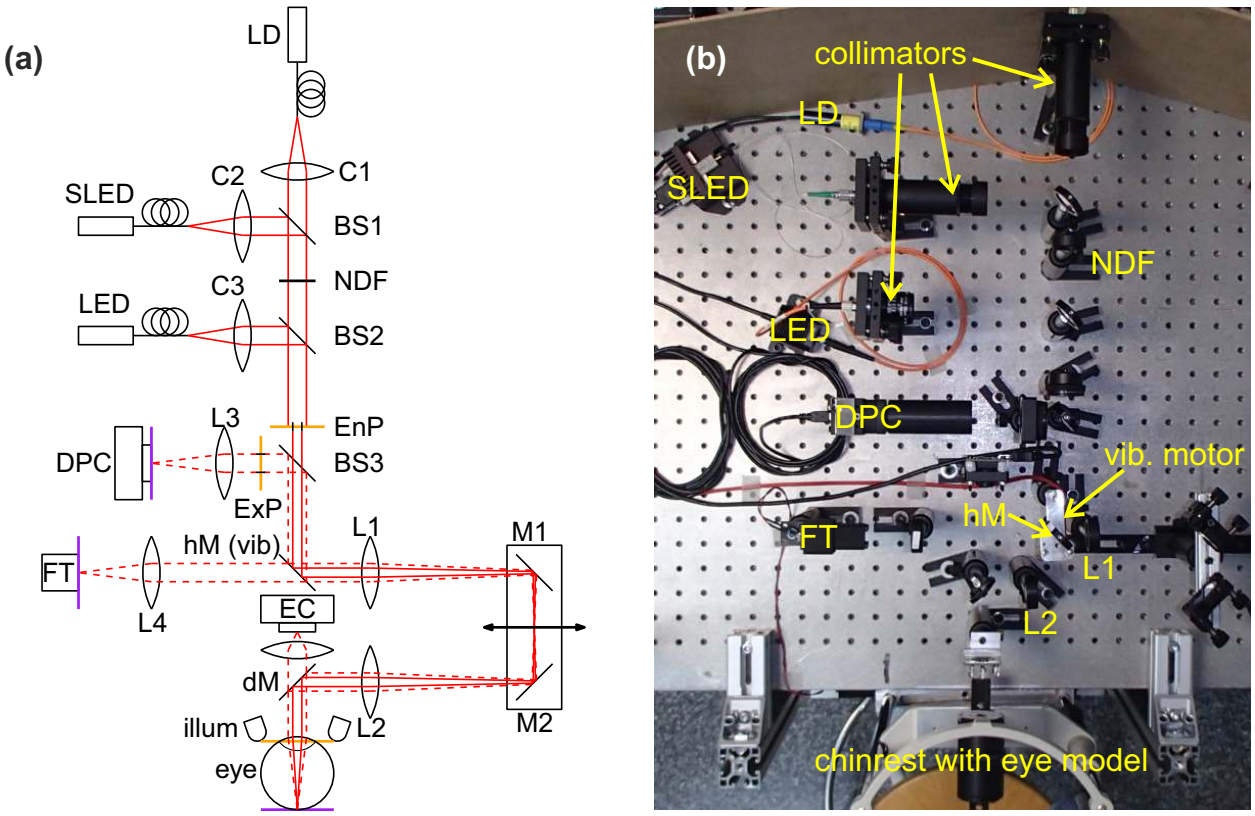

Figure 2.2: (a) Sketch of experimental setup. A laser diode (LD), a light-emitting diode (LED), and a superluminescent diode (SLED) are fiber-coupled into the optical setup and collimated by collimators C1 - C3. NDF: neutral density filter. BS1 - BS3: 50 % beam splitters, EnP/ExP: entrance/exit pupil, hM: hot mirror (with possibility to vibrate), dM: dichroic mirror, L1 - L4: lenses (L1, L2: $f = 150\,\text{mm}$, L3, L4: $f = 100\,\text{mm}$) FT: fixation target, DPC: double pass camera, EC: eye camera, illum: eye illumination, eye: artificial eye. (b) Photo of the setup.

eye, relative to the light beam. During positioning, the eye was illuminated with 940 nm LEDs (illum), which can pass the dichroic mirror (dM) to reach the eye camera (EC).

The entrance pupil (EnP) and exit pupil (ExP) of the system have diameters of 2 mm and 4 mm, respectively, and can be changed by a diaphragm wheel. Both the EnP and ExP are placed in a plane conjugated to the pupil plane (marked in orange). We chose an entrance pupil diameter of 2 mm as a compromise between limiting the diffraction observed for smaller diameters and reducing the effect of aberrations of real eyes when using larger diameters [75]. After EnP, the intensity profile of the beam is approximately flat, which we checked with a camera (IDS UI-1240SE-M) at the pupil plane of the eye.

According to [76], to reach diffraction limit with a 2 mm entrance pupil, visual correction has not only to be performed for defocus, but also for astigmatism. Since we are mainly interested in determining the amount of speckle in our DP images, and use a model eye with negligible spherical and cylindrical aberrations, we do not consider the correction of astigmatism here.

After its second pass in reverse direction through the eye and through the Badal system, the light beam is coupled out by a beam splitter, BS3 (50 %), and imaged by a lens of $f' = 100$ mm focal length onto a CMOS camera (DPC, IDS UI-1240SE-M, 5.3 µm × 5.3 µm pixel size). All measurements were performed with the same exposure time of 500 ms which was chosen in order to fill the dynamic range of the camera, even with the least powerful of the sources, the LED. In the measurements performed with the model eye, the power of the LD and the SLED were adjusted by the driving current and a neutral density filter (NDF, absorbance = optical density 2), in order to provide similar power as the LED at the corneal plane, i.e. ∼0.02 µW.

2.3 Quantification of the speckle in DP images

The speckle contrast, C, (see subsection 1.3.1) is a useful quantifier for speckle patterns with some overall spatial homogeneity (like the pattern in Fig. 1.20), but DP images consist of a relatively narrow intensity distribution localized in the center of the image that is superimposed by speckle as shown in Fig. 2.3. As a consequence, the speckle contrast calculated according to equation 1.28 would be influenced by the specific DP image intensity distribution.

Thus, assuming PSF azimuthal symmetry, we calculate the radial variation of the speckle contrast [68], as shown schematically in Fig. 2.3(f): $C(r) = \sigma_I(r)/\langle I(r)\rangle$, where $\sigma_I(r)$ and $\langle I(r)\rangle$ are computed along a circle of radius r, centered at the centroid of the intensity distribution.

In addition, for each image we perform the following analysis aimed at removing the PSF and the constant part of the background noise before computing the speckle contrast: for all pixels at distance r from the center, we determine the minimum intensity value, $I_{min}(r)$, and obtain a new image by subtracting $I(r) - I_{min}(r)$ (we use the minimum instead of the average to avoid negative values). Then, we calculate the speckle contrast in the central square of the image where speckle

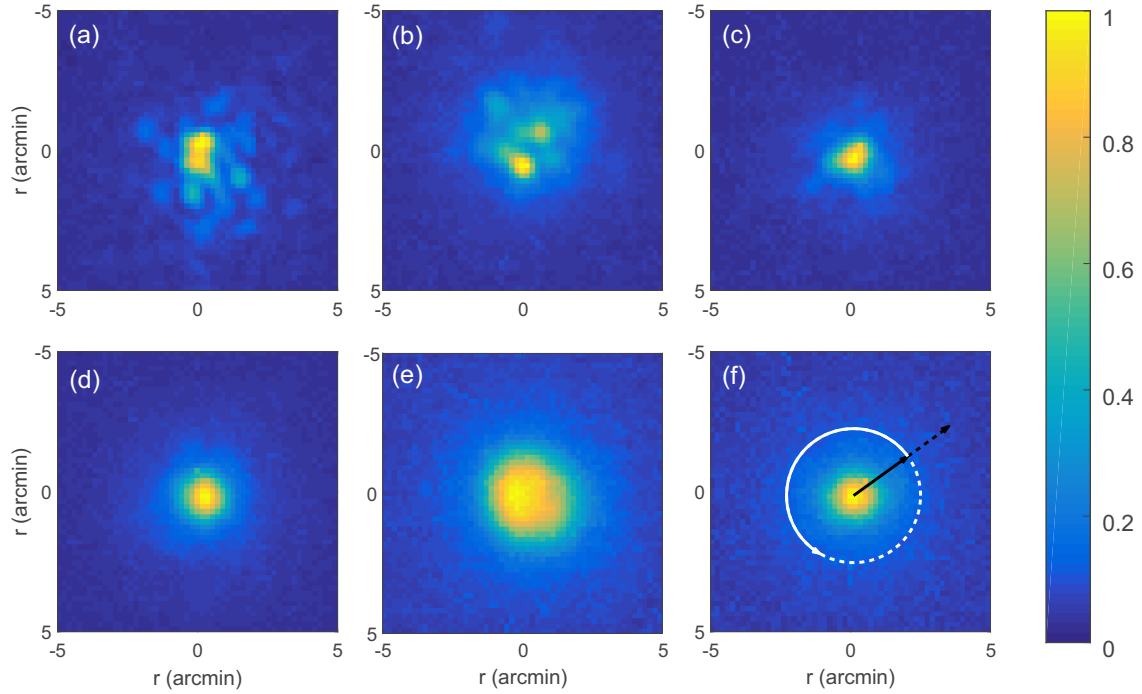

Figure 2.3: Point spread functions (PSFs). The color represents the intensity measured by the double pass camera (DPC in Fig. 2.2), normalized by the maximum value in each image. (a, d) LD, (b, e) LED, (c, f) SLED. Upper row: The vibration of the hot mirror (hM in Fig. 2.2) is turned off, and speckle patterns are observed on the images. Lower row: speckle is reduced when the vibration of the hot mirror is turned on.

is concentrated (41 × 41 pixels [uneven number because we found the central pixel as the centroid of the intensity distribution and we symmetrically consider the same number of pixels around the central pixel in each direction]), C_3, and in a larger region (181 × 181 pixels), C_4, where the speckle contrast measure is more affected by non-constant background noise.

2.4 Results

We present results of DP imaging of a model eye and speckle formation using three light sources (LD, SLED and LED).

Figures 2.3(a–c) display DP images obtained with the LD, the LED and the SLED, without further means of speckle reduction, while Figs. 2.3(d – f) display the DP images obtained using the same model eye and light sources, and turning on the vibration of the hot mirror. The DP images show that speckle formation is reduced by the vibration. Speckle is especially visible in the case of LD without the vibration, Fig. 2.3(a). As expected, speckle formation decreases when a spectrally broader source is used.

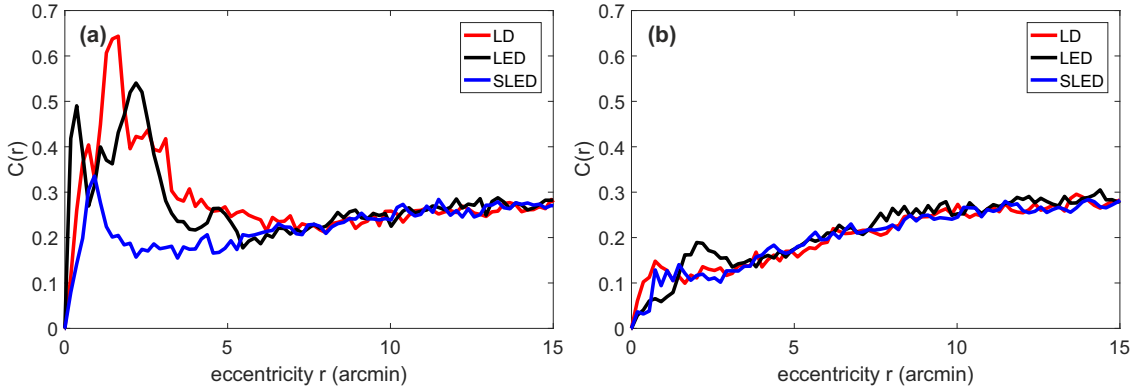

Figure 2.4: Radially evaluated speckle contrast (dimensionless) when the vibration of the hM mirror is turned off (a) and when it is turned on (b).

The radially determined speckle contrast (see section 2.3), $C(r)$, is shown in Figs. 2.4(a) and (b) without and with the vibrating mirror, respectively. Since there is only one pixel in the center of the PSF (and thus no variance), $C(r = 0) = 0$. While for small r the form of the curve depends on the shape of the speckle pattern overlying the PSF, for large r the value of the plateau is determined by the background noise. We attribute the peaks between $r = 0$ arcmin and $r = 5$ arcmin, especially visible in Fig. 2.4(a) to speckle.

In Fig. 2.4(b) we see that speckle is reduced to a similar degree for the three light sources when the vibrating mirror is used. In order to have a scalar quantifier, we compute the area under the curve from pixel 0 to 39 (that corresponds to $r_0 = 7$ arcmin), which is when the lines of the different measurements take similar values, i.e., the start of the plateau. We refer to this index as C_1. To verify that this approach gives consistent results, we also integrated $C(r)$ over pixels 0 - 83 (i.e., up to $r = 15$ arcmin). We refer to this index as C_2.

The values of C_1 and C_2 are listed in Table 2.1. Higher/lower values are due to more/less speckle present in the images. The case of the LD without mirror vibration shows the largest values because speckle is neither reduced by mirror vibration nor by broad band light. With the vibration on, we note that the three light sources cause a similar amount of speckle. Comparing the C_2 values obtained with vibration, we see that the C_2 value obtained with the LED is slightly higher than the C_2 value obtained with the LD and SLED. This is likely due to the fact that the PSF of the LED is wider [see Fig. 2.3(e)]. Comparing the C_1 or C_2 values for SLED with no vibration and for LD with vibration, we can see that they are similar, which suggests that the SLED could be a good all-optical speckle-reduction solution, alternative to the vibrating mirror.

The analysis of the DP images after removing the PSF and the background noise (see section 2.3) confirms this observation: both parameters, C_3 and C_4, indicate that the SLED with no vibration is almost as good as the LD with vibration. We note here high values for the LED without vibration, which we interpret as an artifact due to the fact that, in the DP image, the intensity does not have

	no vibration			vibration		
	LD	LED	SLED	LD	LED	SLED
C_1	2.3	2.1	1.3	1.0	1.0	1.0
C_2	4.3	4.1	3.3	3.0	3.2	3.0
C_3	1.1	3.4	1.0	0.9	0.8	0.7
C_4	1.1	1.8	0.7	0.7	0.6	0.5

Table 2.1: Speckle quantification in the DP images; without/with mirror vibration. $C(r)$ is integrated up to the limit of 7 arcmin, C_1, and up to 15 arcmin, C_2. After flattening the main PSF (see section 2.3) and subtracting the constant background, C is calculated in a square of 41 × 41 pixels (-3.7 to 3.7 arcmin), C_3, and in a square of 181 × 181 pixels (-16.3 to 16.3 arcmin), C_4.

a well-defined center of mass [see Fig. 2.3(b)].

In order to investigate how the information extracted from the DP image (and used for diagnosis) is affected by the amount of speckle, we calculated the MTF for the three light sources with the vibrating mirror on or off by Fourier-transforming the DP image. In the Fourier domain around zero spatial frequency, a peak appears, originating from a DC offset of the image due to retinal and ocular scattering of the model eye and other stray light, as well as camera noise. Therefore, the MTF values at other frequencies are scaled down. To evade this problem, we follow the method used in [6, 77], and replace the first two points of the MTF (up to 1.3 cyc/deg) by fitting the sum of two exponential functions, $f(\nu) = C \cdot \exp(-A\nu) + D \cdot \exp(-B\nu)$, with four parameters, to the remaining MTF data. An alternative for removing the DC peak is subtracting a constant background veil from the image before calculating its Fourier transform [65].

To compare the MTFs, we first selected a benchmark measurement (as in [68], we use the DP image recorded with the laser and the mirror vibrating). Then, we determine the relative difference of the MTF of a given configuration (M_x), as a function of the spatial frequency ν:

$$e_{\mathrm{M}}(\nu) = \frac{\mathrm{M}_x(\nu) - \mathrm{M}_b(\nu)}{\mathrm{M}_b(\nu)}, \tag{2.1}$$

where M_b is the benchmark MTF.

The results are presented in Fig. 2.5. Figure 2.5(a) shows the results for the measurements where the vibrating mirror was not used. The positive relative variations at higher frequencies are due to speckle present in the images. In Fig. 2.5(b), we see that when using the vibrating mirror, the relative variation is negative, because the vibrating mirror reduces the speckle. The red line, representing the LD, stays at zero because it is used as the benchmark. In both graphs, the MTF relative variation of the LED is negative (except in Fig. 2.5(a) at high frequencies). This is because the LED can not be considered a point source as narrow as the other sources, leading to a wider

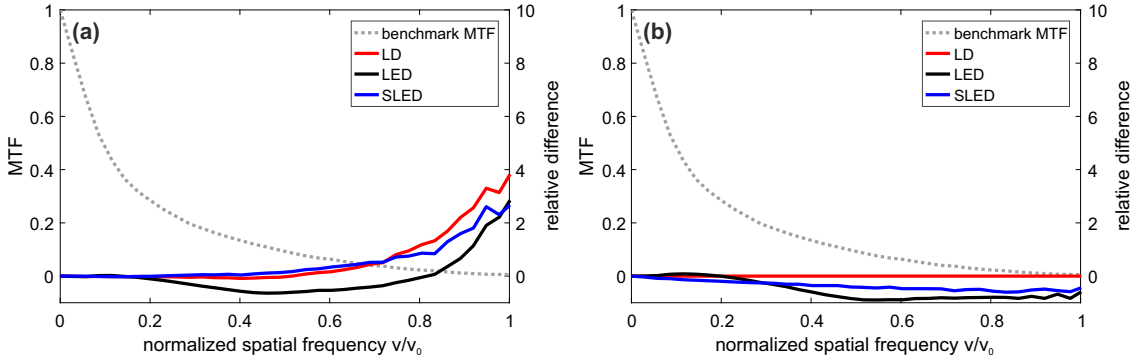

Figure 2.5: Benchmark MTF, depicted by gray dotted line (corresponding to the left vertical axis), obtained by using the LD as light source and employing the vibrating mirror. The frequency axis is normalized by the diffraction limited cutoff frequency, $\nu_0 = 44.75$ cyc/deg. The blue, red, and black line correspond to the right vertical axis, showing the relative difference of the MTFs (equation 2.1) of LD, LED and SLED to the benchmark MTF, without (a) and with (b) mirror vibration. In panel (b) the red line stays at zero because the LD with mirror vibration is used as the benchmark.

PSF, as shown in Fig. 2.6. The higher relative differences of the MTFs at higher normalized spatial frequencies in the case without the vibrating mirror (Fig. 2.5(a)) might be due to the roughness of the cardboard that acts as the retina in our model eye. For real eyes, the retinal cone spacing between 3 to 8 micrometers corresponds to spatial frequencies close to the cutoff frequency [72, 78–80].

2.5 Discussion

We have performed a comparative study of the amount of speckle in DP images of a model eye by using an LD, an LED or an SLED as light source, with and without vibration of a mirror in the beam path. Our setup permits to switch between light sources without the need for realignment, thus offering an objective comparison of DP images.

We have found that, when the mirror vibration is turned on, the three light sources yield very similar amounts of speckle. With the vibration turned off, the SLED gave a degree of speckle close to, but slightly higher than the degree of speckle obtained with the LD with vibrating mirror. The reduced speckle contrast of the SLED in comparison to the LD is due to its broader optical spectrum, which corresponds to a shorter coherence length of the light. Therefore, it can be an all-optical solution for speckle reduction in DP imaging, avoiding undesirable mechanical vibrations. The similar spectral widths of SLED and LED suggest comparable performance regarding speckle reduction. However, the light of the LED is difficult to collimate and experiences large losses when coupled to our setup by fiber, to the point of being too weak to obtain measurements of real eyes

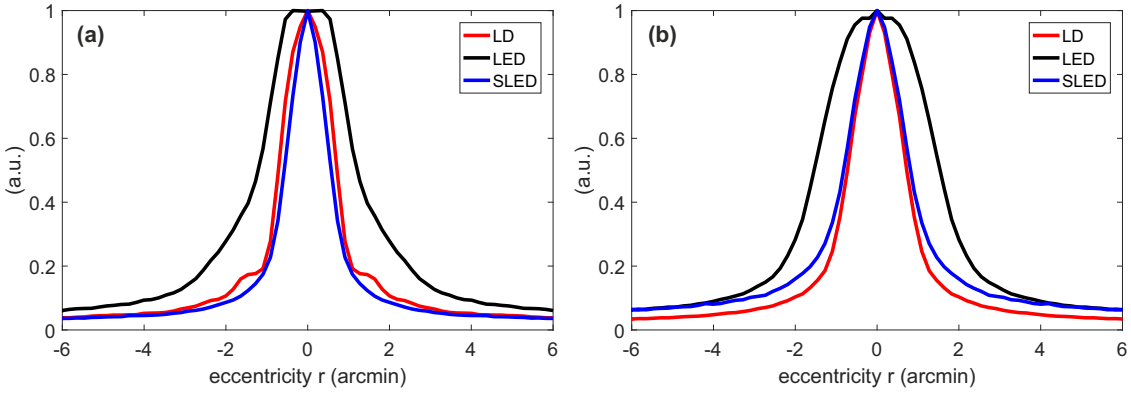

Figure 2.6: Radial profile of the PSF when the vibration of the mirror hM is turned off (a) and when it is turned on (b).

because of the required long exposure time. The SLED has a number of drawbacks, too: it is more expensive than the LD, and it does not reduce speckle to the extent of the LD with vibrating mirror.

The impact of longitudinal chromatic aberrations and diffraction on the DP images, corresponding to the light sources tested in this study, is negligible, as all them have peaks in the near infrared and limited spectral bandwidth (on the order of 50 nm for the LED and the SLED). In fact, differences of less than 1 pixel in the widths of the PSFs are expected from simulations.

3 The effect of optical feedback and pump current modulation on speckle

The temporal coherence of a light source can be reduced by inducing optical chaos. In this chapter, we use optical feedback and current modulation to experimentally induce optical chaos in a LD and determine the effect on speckle patterns generated by this light. Our experiments show a decrease of the speckle contrast using this method.

Results of this chapter have not been published.

3.1 Introduction

Optical feedback and pump current modulation are two possibilities to induce chaotic behavior in LDs [38]. Two important properties of chaos are aperiodicity and sensitive dependency to initial conditions. Depending on the feedback regime and the phase of the optical feedback, the laser linewidth can be either narrowed or broadened [36]. In the coherence collapse (regime IV), optical feedback clearly increases the linewidth [81]. This effect has been used to reduce speckle in microscopy [61].

Here, we study the effect of optical feedback and pump current modulation on the linewidth broadening and discuss possible application for speckle reduction in DP imaging.

3.2 Experiments

3.2.1 Optical feedback

In the optical feedback experiment, we use the setup sketched in Fig. 3.1. A mirror (M1) in the laser beam path defines an external cavity ($L_{\mathrm{ext}} = 50\,\mathrm{cm} \Rightarrow \tau \approx 3.5\,\mathrm{ns}$) and a beam splitter is used to couple light out for measurements. We use an LD (Hitachi HL6501MG) with a wavelength of $\lambda = 656\,\mathrm{nm}$ and threshold current around $J_{\mathrm{p,thr}} = 39.5\,\mathrm{mA}$. Light from the LD is sent through a step-index multimode optical fiber with a core diameter of $200\,\mu\mathrm{m}$ (Thorlabs M72L02) and the light exiting at the other end is imaged by a 8-bit CMOS camera (IDS UI-1240SE-M). Speckle is created by interference of different guided modes in the fiber. We also measure the spectrum of the light using an optical spectrum analyzer (OSA, Anritsu MS9710C).

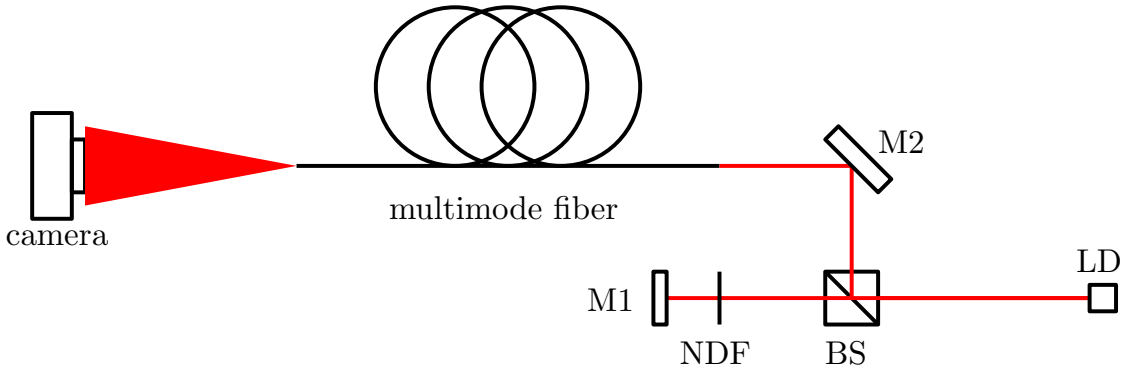

Figure 3.1: Setup of the optical feedback experiment. The optical density of the neutral density filter (NDF) and the transmission of the beam splitter (BS) determine the amount of feedback. M1, M2: mirrors.

3.2.2 Pump current modulation

We use a LD with a wavelength of $\lambda = 685\,\mathrm{nm}$ (Thorlabs HL6750MG) and threshold current around $J_{\mathrm{p,thr}} = 26.7\,\mathrm{mA}$. We drive it at $J_{\mathrm{p}} = 30\,\mathrm{mA}$ and apply a square wave modulation current of $\pm 15\,\mathrm{mA}$ (using an arbitrary waveform generator, Agilent 81150A) such that the LD is turned off and on in each cycle. We choose a modulation frequency of $f_{\mathrm{mod}} = 200\,\mathrm{Hz}$ such that with a camera exposure time of $t_{\mathrm{exp}} = 50\,\mathrm{ms}$ a photo of the speckle pattern contains 4 full modulation cycles. We repeat the measurement with $f_{\mathrm{mod}} = 200\,\mathrm{kHz}$.

As in the feedback experiment, speckle is created inside the multimode optical fiber and imaged with the camera. At the same time, the spectrum is recorded by the OSA.

3.3 Results

3.3.1 Optical feedback

The power curves without and with optical feedback are shown in Fig. 3.2. According to equation 1.20, we have a feedback-induced threshold reduction of 16.4 %.

Figure 3.3 and Fig. 3.4 show the spectra of the LD as a function of the pump current without and with optical feedback, respectively.

Without feedback we see one dominant mode at all pump current. The wavelength of the modes increases slightly with increasing pump current. At certain pump currents we observe mode hopping, i.e. jumps between longitudinal lasing modes. In the case with feedback, several longitudinal lasing modes have similar power and thus these features are not as visible. The spectra are wider for all pump currents. However, the spectral width (better visible in the single spectra in Fig. 3.5) increases from $\Delta\lambda_{FWHM} \approx 0.1\,\mathrm{nm}$ to $\Delta\lambda_{FWHM} \approx 1.5\,\mathrm{nm}$ when optical feedback is

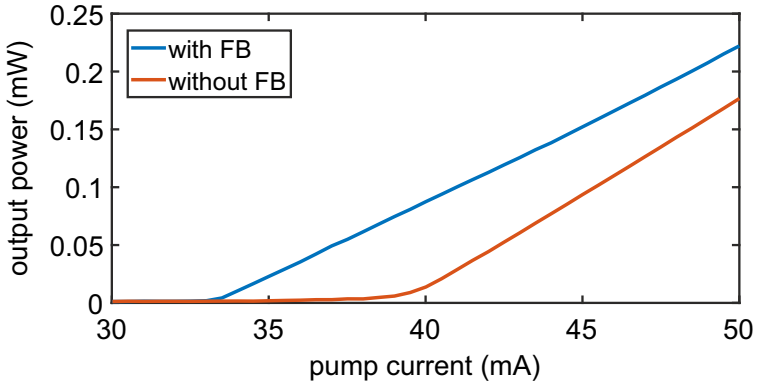

Figure 3.2: Power curves of the LD with and without optical feedback.

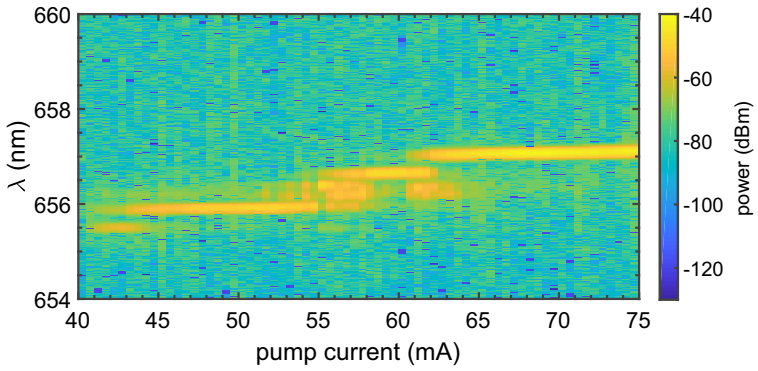

Figure 3.3: Optical spectrum of the laser diode without feedback as a function of the pump current.

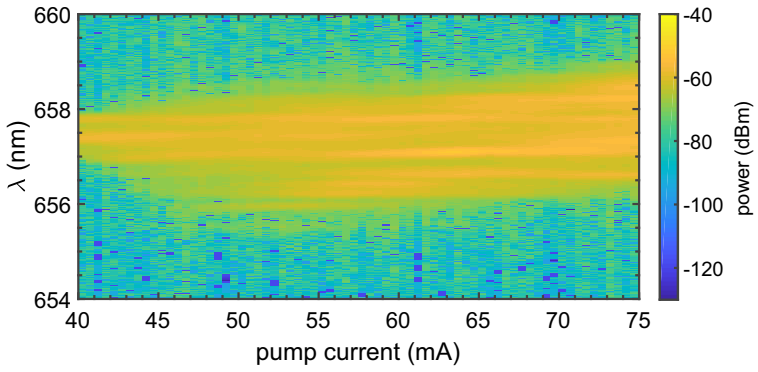

Figure 3.4: Optical spectrum of the laser diode with feedback as a function of the pump current.

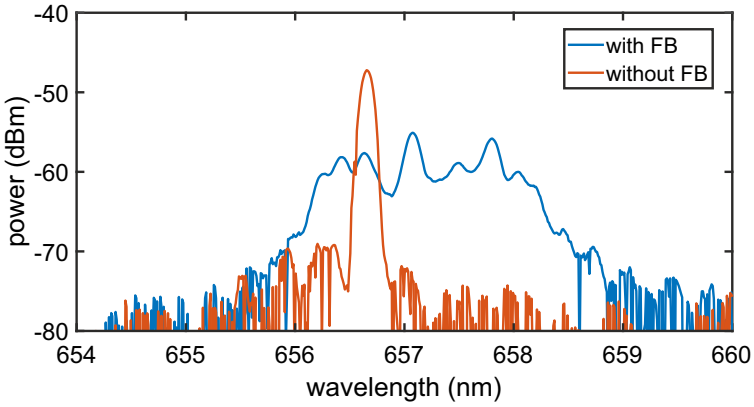

Figure 3.5: LD spectra without and with optical FB taken at a pump current of $J_\mathrm{p} = 60\,\mathrm{mA}$.

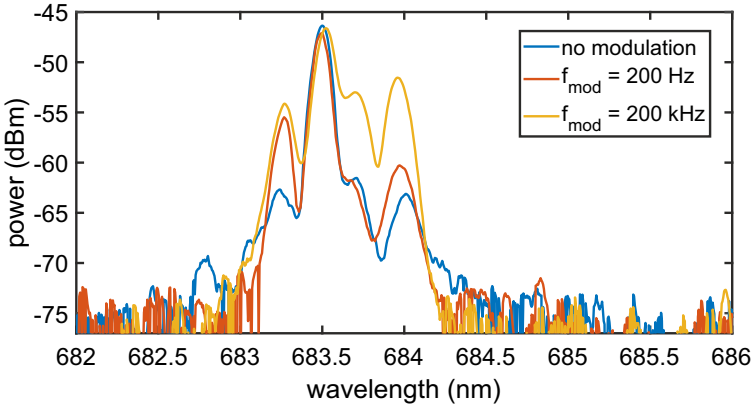

Figure 3.6: LD spectra without and with current modulation ($f_\mathrm{mod} = 200\,\mathrm{Hz}$ and $f_\mathrm{mod} = 200\,\mathrm{kHz}$).

induced.

We measure the speckle contrast in a circular area in the center of the speckle image (radius $r = 200$ pixel). In this way we make sure there is no large variation of the mean intensity across the analyzed area and intensity variations are mainly due to speckle.

The speckle contrast is reduced from $C = 0.44$ to $C = 0.18$ if optical feedback is induced. This corresponds to a relative speckle contrast reduction $(C_0 - C_\mathrm{red})/C_0$ of 58 %. C_0 is the speckle contrast produced by coherent laser light ("solitary" LD without feedback), and C_red is the reduced speckle contrast produced by spectrally broadened laser light (LD with optical feedback).

3.3.2 Pump current modulation

The broadening of the spectrum by current modulation is very small and only slightly affects the height of the side modes as shown in Fig. 3.6. It is not measurable in terms of $\Delta\lambda_{FWHM}$.

Measuring the speckle contrast in a circular area as in the feedback experiment, we obtain speckle

contrast reduction from $C = 0.53$ in the case without modulation to $C = 0.34$ for $f_{\mathrm{mod}} = 200\,\mathrm{Hz}$ and $C = 0.41$ in the case of $f_{\mathrm{mod}} = 200\,\mathrm{kHz}$. The relative speckle contrast reduction is 23 % and 36 %, respectively.

3.4 Discussion

A spectral broadening of $\Delta\lambda_{FWHM} \approx 1.5\,\mathrm{nm}$ is achieved by optical feedback. When imaging the speckle created inside a multimode optical fiber, we obtain a reduction of speckle contrast of 58 %.

When we modulate the pump current of the laser diode with $f_{\mathrm{mod}} = 200\,\mathrm{Hz}$, we observe a very slight broadening of the optical spectrum. The speckle contrast is reduced by 23 % (36 %) for a modulation frequency of $f_{\mathrm{mod}} = 200\,\mathrm{Hz}$ ($f_{\mathrm{mod}} = 200\,\mathrm{kHz}$).

The amount of speckle reduction achieved by these methods can be partially explained by the broadening of the optical spectra.

Since the broadening is relatively small, we speculate that fast variations of the optical spectrum not measurable with our setup play a role in the speckle reduction. The optical spectrum analyzer records on the order of 10 s for a measurement at highest spectral resolution.

In future work it can be interesting to map in detail the speckle reduction as a function of the current modulation parameters amplitude and frequency as well as the effect of the exposure time. Moreover, the fast variations of the optical spectrum can be further investigated.

4 Speckle contrast as a function of laser diode pump current

Speckle patterns produced by coherent waves interfering with each other are undesirable in many imaging applications (e.g. DP imaging), but on the other hand, they contain useful information that can be exploited in a number of applications (see section 1.3 for examples). Therefore, it is interesting to enhance or reduce speckle by tailoring the coherence of light. In this chapter, we use a conventional semiconductor laser and a multimode optical fiber to study experimentally how a speckle pattern depends on the laser pump current and on the image acquisition settings.

Results of this chapter have been published in [82].

4.1 Introduction

A light source for DP imaging should emit light in the visible wavelength range, i.e. between red and blue. In particular, if narrow-banded, a green light source would be the most representative because the eye is most sensitive at this color (see Fig. 4.1). On the other hand, considering the intensity needed for DP imaging, the high sensitivity at $\lambda \approx 550\,\text{nm}$ makes patients suffer from glare. For this reason, near-infrared light is frequently used, even though corresponding DP images show larger scattering [18, 83, 84]. The light source should furthermore offer a highly directional beam providing at least many hundreds of microwatts of power (so that several tens of microwatts can reach the corneal surface through the DP system).

As speckle contrast increases when the spectral width of the source decreases [44], we seek to use a source with a relatively broad spectrum to minimize speckle. However, since we only care about monochromatic aberrations, the width of the source's spectrum is limited. Possible chromatic aberrations would lead to an underestimation of the MTF of the eye measured with a DP system [74]. In addition, the source should be of low cost. A superluminescent diode meets the other requirements [70, 73], but its cost prevents its use in inexpensive DP instruments.

Alternative approaches for reducing speckle in DP imaging include the use of acoustic modulation of laser beams [67] or the periodic variation of the vergence of a lens in the light beam [68] (but these are not low cost solutions), or by mechanical means: employing a vibrating mirror for scanning the beam [69] is a low cost solution, but introduces undesired mechanical vibrations in the setup.

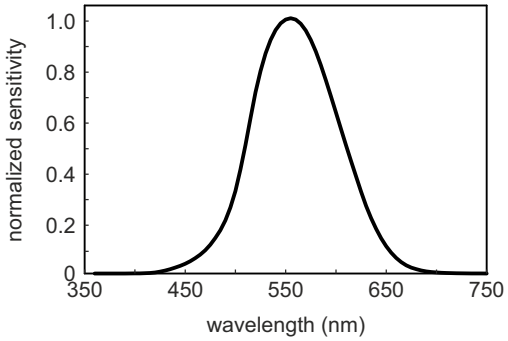

Figure 4.1: Spectral sensitivity of the photometric observer (photopic luminosity function). It represents the perception of brightness as a function of wavelengths. After [85].

An all-optical approach for speckle reduction includes broadening the spectrum through optical feedback [61]; however, the broadening is limited by the gain bandwidth of the semiconductor material and is not sufficient to obtain a significant speckle reduction. Other approaches are based on the introduction of a disordered material in the laser cavity to facilitate multiple scattering [57], or the use of specially designed cavities [86, 87] (see [88] for a recent review). The drawback of these approaches for use in DP imaging systems is that they are not commercially available.

An alternative strategy that we examine here is the possibility of controlling the amount of speckle produced by semiconductor laser light by tuning the laser pump current across the lasing threshold.

Below the threshold the emitted light is mainly due to spontaneous emission and thus of low coherence. When the pump current, J_p, is increased above the threshold, the emitted light becomes coherent due to stimulated emission and the linewidth of the spectrum decreases. A multimode fiber generates apparently random speckle patterns [86]. When a laser source is used with a spectrum that contains a large number of narrow longitudinal modes, patterns with high speckle contrast can be obtained [62, 63]. Here we use a multimode semiconductor laser and a multimode fiber to generate speckle patterns and analyze how the amount of speckle depends on the laser current. Because below the threshold the intensity is very low, we also need to adjust the exposure time of the camera, t_exp. Thus, we vary (J_p, t_exp) in the range of values that permit to record images with sufficient intensity, but preventing overexposure.

Our goal is to find pairs (J_p, t_exp) that allow recording images with similar average intensity, but with different amount of speckle.

4.2 Experiment

Figure 4.2(a) describes the experimental setup. We use a semiconductor laser diode (Thorlabs HL6750MG, the same one as in subsection 3.2.2) based on a AlGaInP multi-quantum well structure

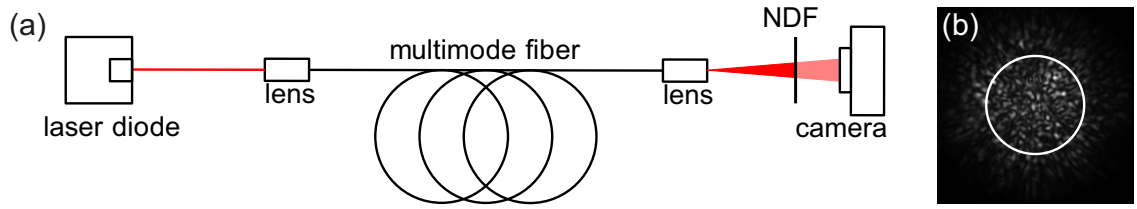

Figure 4.2: (a) Experimental setup. NDF: neutral density filter of optical density 1.7. (b) Example speckle image with the area where the speckle contrast is computed indicated with a white circle.

with nominal wavelength $\lambda = 685\,\text{nm}$, and threshold current of approximately $J_{\text{p,thr}} \approx 26.7\,\text{mA}$ at 18 °C. Speckle is created by a step-index multimode fiber with a core diameter of 200 µm (Thorlabs M72L02) by interference of different guided modes [62, 86]. We record the intensity at the end of the fiber with a 8 bit CMOS camera (IDS UI-1240SE-M). The laser pump current, J_p, and the exposure time, t_exp, are control parameters that are varied within the range of values that permit recording images whose brightness is not too low, nor overexposed. A neutral density filter (NDF) used during all measurements ensures that the shortest possible exposure time of the camera is sufficient to obtain non-overexposed images at high pump currents.

The amount of speckle is quantified by the speckle contrast, $C = \sigma_I/\langle I\rangle$, where σ_I is the standard deviation of the intensity and $\langle I\rangle$ is the mean intensity. To minimize the influence of the non-uniformity of the intensity distribution, we calculate C inside the circular central area of radius 200 pixels, as shown in Fig. 4.2(b), which encloses approximately 125000 pixels with values in the range [0-255]. In this way, we disregard the outer part of the image. We have verified that the results are robust to the size of the area: a similar variation of C with the laser pump current and with the camera exposure time was found when considering radius of 150 or 250 pixels. We ensure that the size of the imaged speckle spots is larger than several camera pixels in order to avoid pixel averaging [59].

4.3 Results

First we examine the optical spectra (measured with a 4 nm spectral resolution spectrometer, Photoresearch PR655) of the laser when it is pumped at various pump currents from below to above threshold, as shown in Fig. 4.3(a). Below threshold, the estimated linewidth (full width half maximum) is about 19 nm (see inset). In Fig. 4.3(b) we show in color code the spectrum of the laser (measured with the OSA, Anritsu MS9710C), as a function of the pump current. We see that above the threshold several cavity modes turn on (yellow lines) and the emission becomes nearly monomode at higher pump currents.

We recorded images of speckle patterns at pump currents from $J_\text{p} = 16\,\text{mA}$ (below the lasing

threshold) up to 44 mA (single-mode emission) using different exposure times for each pump current value (for most pump currents, at least five images with different exposure times were taken). The criterion used to determine the range of exposure times is the same for all pump currents: we selected t_{exp} such that the images were neither overexposed (i.e. had no pixel with the maximum digital value of 255), nor of very low intensity (we disregarded images where the pixels within the circle had an average digital value < 10 in order to avoid quantization effects and possible dominance of noise).

The white dots on top of the spectral map, Fig. 4.3(b), represent the mean speckle contrast, $\langle C \rangle$, averaged over the speckle contrast from images obtained with different exposure times, and the error bars represent one standard deviation. We see that below $J_{\mathrm{p}} \approx 24\,\mathrm{mA}$ $\langle C \rangle$ is small ($\langle C \rangle \approx 0.16$) and only slightly increases with the pump current. Between $J_{\mathrm{p}} \approx 24\,\mathrm{mA}$ and 30 mA, coinciding with the lasing threshold, $\langle C \rangle$ increases strongly, whereupon the increase flattens and reaches a plateau of $\langle C \rangle \approx 1$ at 42 mA. The increase of C does not happen instantaneously when tuning the pump current from below to above threshold because first several modes start lasing before the output changes to single-mode at around $J_{\mathrm{p}} \approx 40\,\mathrm{mA}$. The variation of the speckle contrast for images taken with different exposure times (represented by the error bars in Fig. 4.3(b)) is negligible at low and high pump currents. However, for an intermediate range of pump currents ($29\,\mathrm{mA} < J_{\mathrm{p}} < 40\,\mathrm{mA}$), there is more variability (larger error bars), which we attribute to the competition of the laser cavity modes, which create different realizations of speckle patterns for the same pump current. The shape of the plot of C vs J_p in log-log scale (not shown) is similar to the input-output characteristic of the laser, but does not show the same saturation behavior at low pump currents, perhaps due to the limited sensitivity of the camera

Figure 4.4 shows the speckle contrast computed from all the individual images recorded, as a function of the mean intensity of the image. In Fig. 4.4(a), the color indicates the value of the pump current, in Fig. 4.4(b), the exposure time. The highest mean intensities correspond to low speckle contrast values, i.e., relatively homogeneous patterns that originate from low coherence light at pump currents under the lasing threshold, which are recorded with a relatively long exposure times of the camera ($t_{\mathrm{exp}} = 5\,\mathrm{ms} - 60\,\mathrm{ms}$). At lower mean intensities, a large range of speckle contrasts can be achieved for a constant mean intensity by adjusting both the pump current and the exposure time. The highest speckle contrast values ($C \approx 1$) occur for $\langle I \rangle < 30$.

In Fig. 4.5, we present six example images recorded with different pump currents and exposure times, and the corresponding intensity histograms, obtained from the pixel values within the circle. In the first two lines, from top to bottom, the mean intensities of the speckle patterns lie within ranges of $\langle I \rangle \in [40, 50]$ and $\langle I \rangle \in [50, 60]$, respectively. The speckle patterns recorded with the laser current above the threshold (right column) use the full dynamic range of the camera (8 bit, 256 digital gray values). Patterns with approximately the same mean intensity, but taken with the pump current below the threshold (left column) and with much longer exposure times are more

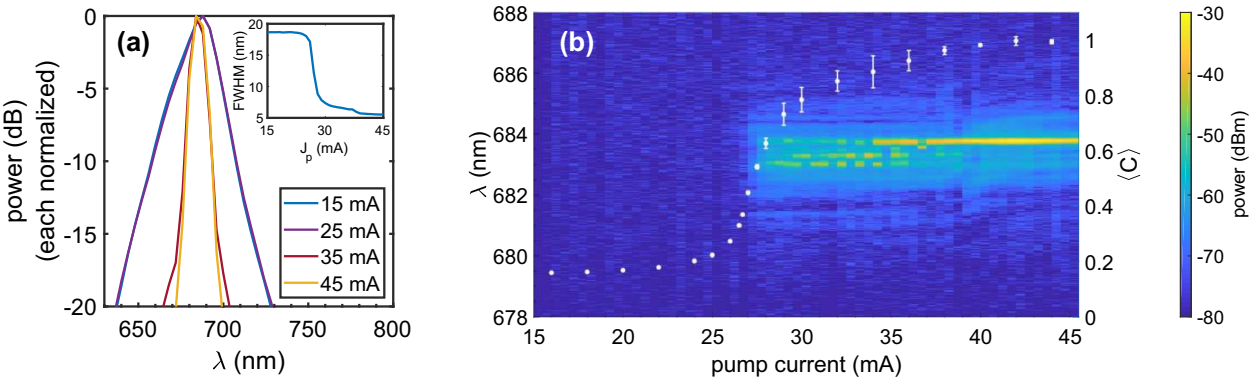

Figure 4.3: (a) Optical spectra recorded at various pump currents (J_p = 15 mA, 25 mA, 35 mA, 45 mA), normalized to the maximum value. The spectra of 15 mA and 25 mA are almost indistinguishable. The inset shows the relationship between pump current and linewidth (full width half maximum). (b) Optical spectrum in color code vs. the pump current. The white dots represent the speckle contrast, averaged over measurements performed with different exposure times. The error bars indicate one standard deviation.

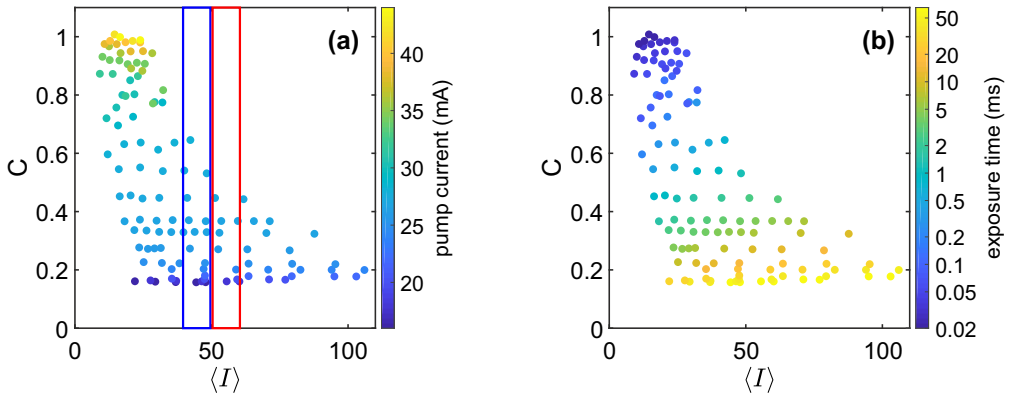

Figure 4.4: Speckle contrast as a function of the mean intensity (in digital levels) for the same data as shown in Fig. 4.3(b). In (a), the color represents the corresponding pump current; in (b), it shows the exposure time.

homogeneous, i.e., have a narrower intensity histogram, and thus lower speckle contrast. In the bottom line of Fig. 4.5, we present the speckle pattern with the highest mean intensity, $\langle I \rangle = 106$ and that with highest speckle contrast, $C = 0.99$, obtained with a pump current of $J_\mathrm{p} = 44\,\mathrm{mA}$.

The two panels in Fig. 4.6 show the values of (J_p, t_exp) used for each speckle measurement. In Fig. 4.6(a), the color of each point represents the mean intensity of the speckle pattern, while in Fig. 4.6(b), the color represents the speckle contrast. We note that, in order to obtain well-exposed images, t_exp needs to be decreased by three orders of magnitude (from $t_\mathrm{exp} = 60\,\mathrm{ms}$ to $0.03\,\mathrm{ms}$) when the pump current is increased from $J_\mathrm{p} = 16\,\mathrm{mA}$ to $44\,\mathrm{mA}$. As it was shown in Fig. 4.4, the highest mean intensities and the lowest speckle contrasts are achieved below the lasing threshold with long exposure times.

In Fig. 4.7, we show for two different intervals of mean intensities, corresponding to vertical windows in Fig. 4.4(a), $\langle I \rangle \in [40, 50]$ (blue window) and $\langle I \rangle \in [50, 60]$ (red window), the plots of t_exp vs. J_p. The color code indicates the speckle contrast and shows that different C values that can be achieved by adjusting t_exp and J_p. The first four images shown in Fig. 4.5 correspond to the lowest and highest pump currents in each of these plots.

4.4 Discussion

We have studied experimentally how the speckle pattern at the output of a multimode fiber depends on the laser pump current and on the image acquisition settings. We have obtained images of speckle patterns with different amount of speckle (speckle contrast $C \approx 0.16 - 0.99$) by tuning the pump current from far below the lasing threshold to far above the threshold, $J_\mathrm{p} = 16\,\mathrm{mA}$ to $44\,\mathrm{mA}$, and we kept the average intensity of the images within an appropriate range of values (to avoid too dark images or overexposed images) by adjusting the exposure time of the camera over three orders of magnitude, from $t_\mathrm{exp} = 60\,\mathrm{ms}$ to $0.02\,\mathrm{ms}$. We have observed a sharp increase in the speckle contrast when the pump current is varied from below to above the threshold. This observation is interesting for applications where speckle needs to be suppressed or enhanced. In particular, if high intensity illumination is not required, or if long exposure times are possible, lowering the pump current under the threshold can be a simple solution for adjusting the amount of speckle.

For speckle reduction in DP imaging, a laser offering higher output power below threshold would be needed. When the laser in our setup is pumped just below the threshold ($J_\mathrm{p} = 24$ mA), it produces an output of 80 microwatts. On the corneal plane, the maximum permissible exposure is a few tens of microwatts, depending on the wavelength. However, due to the optics necessary for improving the beam quality and guiding the light to the eye, only a small fraction of the power from the laser diode will arrive at the eye. Images taken with low power require longer exposure times, which reduces image quality because of unavoidable eye movements of patients.

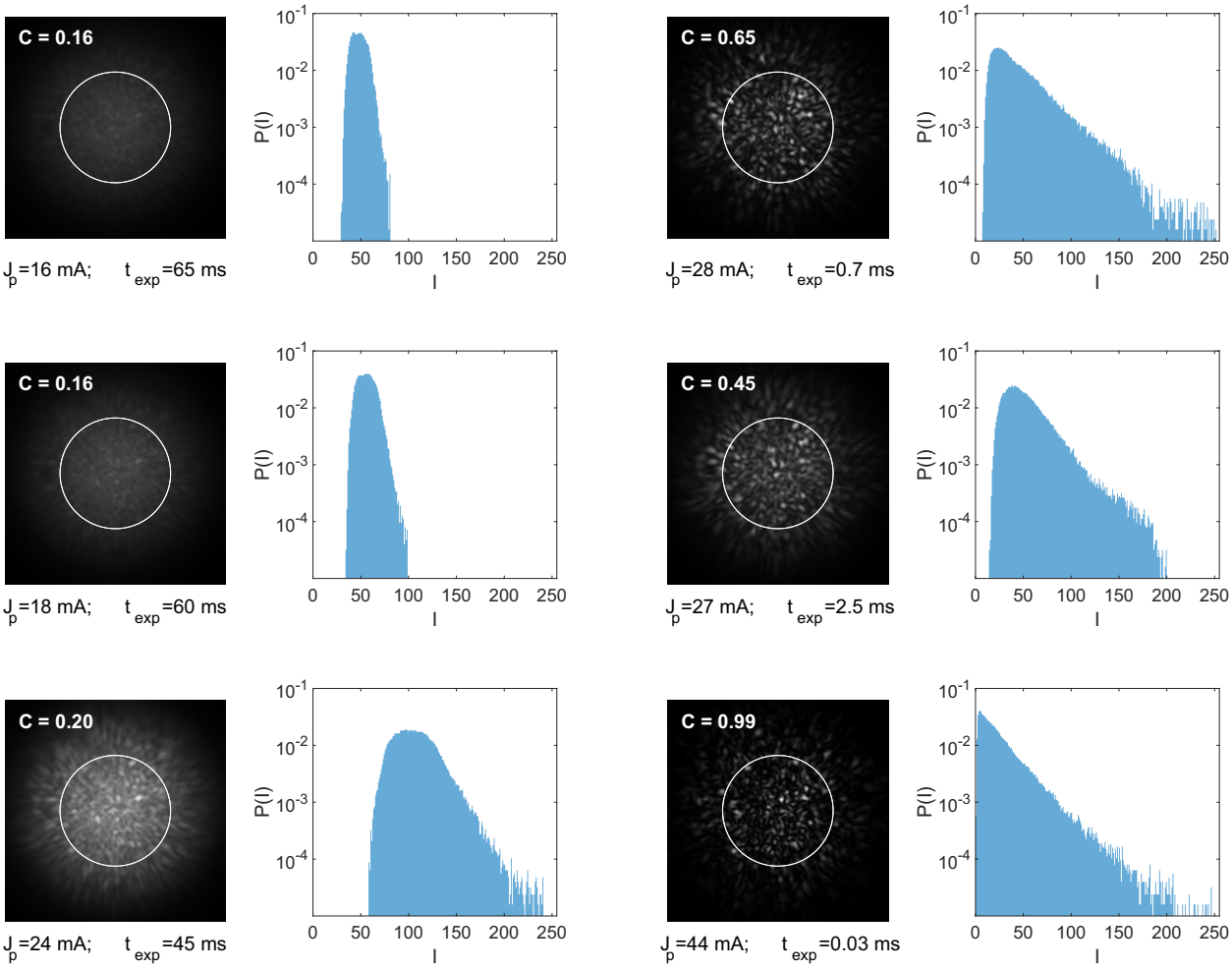

Figure 4.5: Example images and histograms depicting the intensity distribution inside the areas indicated by white circles. In the first two lines from top to bottom, we present images of similar average intensities, within $\langle I \rangle \in [40, 50]$), and $\langle I \rangle \in [50, 60]$, respectively, from low (left column) and high pump current (right column), taken with different exposure times. In the third line, the cases of highest mean intensity ($\langle I \rangle \approx 106$, left column) and highest speckle contrast ($C = 0.99$ and $\langle I \rangle \approx 24$, right column) are shown.

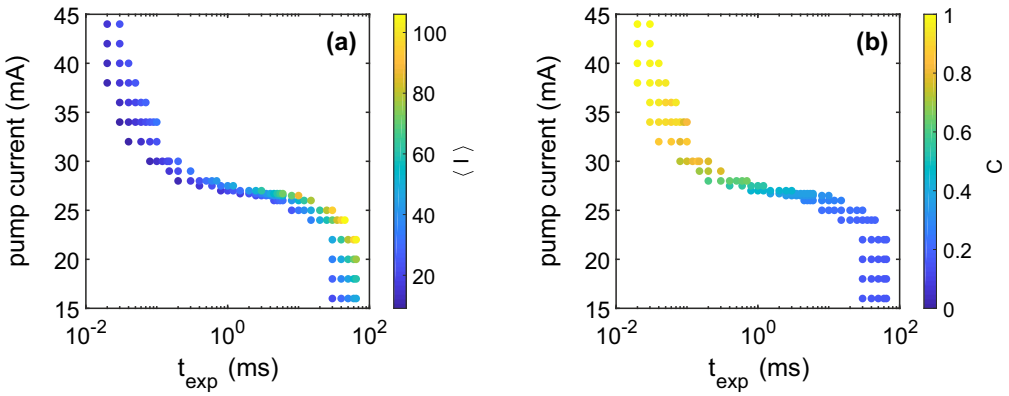

Figure 4.6: Scatter plot of the exposure time and the pump current for all measurements. The color code indicates (a) the mean intensity, (b) the speckle contrast.

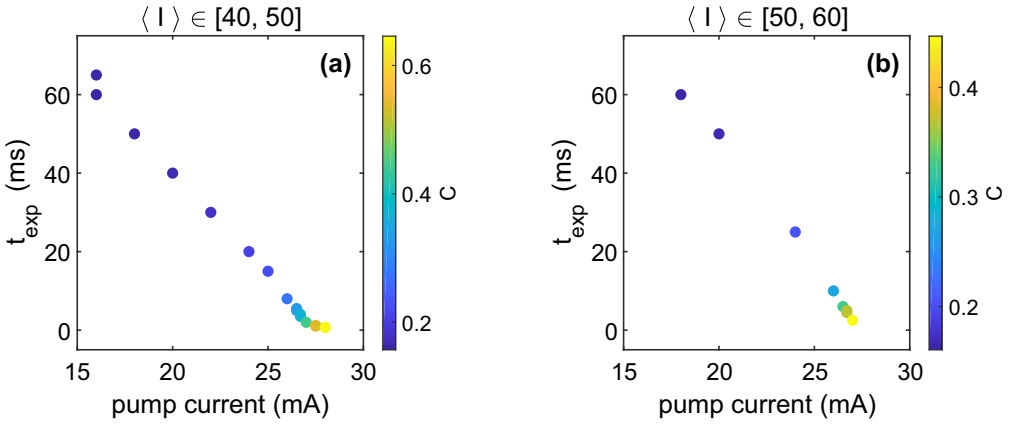

Figure 4.7: Exposure time vs pump current for images that have mean intensity in the range (a) $\langle I \rangle \in [40, 50]$ and (b) $\langle I \rangle \in [50, 60]$. The color code indicates the speckle contrast.

5 Conclusions and future work

5.1 Conclusions

In this thesis we have studied possibilities of a non-mechanical solution for speckle reduction based on a semiconductor light source. Our particular focus has been the applicability in double pass imaging. We can summarize the results presented in this thesis as follows:

In chapter 2 we presented experimental results on speckle formation in DP imaging when using different semiconductor light sources (an LD, an LED and an SLED). We have found that with a vibrating mirror in the beam path, the three light sources yield similar amounts of speckle in DP images, as expected. The SLED without mirror vibration gave a degree of speckle close to, but slightly higher than the degree of speckle obtained with the LD with vibrating mirror. The SLED and LED lead to comparable performance regarding speckle reduction, due to the fact that they have similar spectral widths. The LED is an inexpensive light source, however, its light is difficult to collimate and experiences large losses when spatially filtered or coupled to an optical fiber, to the point of being too weak to obtain DP measurements of real eyes during viable exposure times. The SLED has drawbacks, too: it is far more expensive than an LED or LD, and it does not reduce speckle quite as well as a LD in combination with a vibrating mirror. However, it avoids undesired mechanical vibrations.

In chapter 3 we observed a reduction of speckle (produced by interference of different guided modes in a multimode optical fiber) by optical feedback and by pump current modulation of the LD. With both techniques, we observed a small broadening of the optical spectrum. At the same time, the achieved speckle contrast reduction of up to 58 % in the case of optical feedback is quite large. However, optical feedback and current modulation are not optimal solutions for decreasing speckle in DP imaging instruments because they increase the complexity of the setup.

In chapter 4 we experimentally investigated the amount of speckle at the end of a multimode optical fiber as a function of the pump current applied to a semiconductor laser. We have demonstrated that the speckle contrast can be tuned in a range of $C \approx 0.16 - 0.99$ by changing the pump current from far below to far above threshold ($J_\mathrm{p} = 16$ mA to 44 mA and $J_\mathrm{thr} \approx 26.7\,\mathrm{mA}$ at 18 °C). The speckle contrast increases abruptly when the pump current is increased across the threshold. Adjusting the image acquisition time over three orders of magnitude ($t_\mathrm{exp} = 60\,\mathrm{ms}$ for the lowest current and $t_\mathrm{exp} = 0.03\,\mathrm{ms}$ for the highest current) allowed us to record images that were

well-exposed (neither overexposed, nor dark).

We conclude that for applications in which high intensity illumination is not required, lowering the pump current just under the threshold can be a simple solution for reducing the amount of speckle. In the particular case of DP instruments, the power needed to illuminate the eye is several tens of microwatts at the corneal surface, i.e. the light source should emit several hundreds of microwatts, taking into account losses in the optical system. Therefore, we speculate that an LD that emits this power when pumped close to threshold can be a solution for speckle reduction in DP imaging.

5.2 Future work

The work we have presented here offer several points for continuation. Some of them are:

- In future work it will be interesting to investigate speckle reduction in DP images recorded from real eyes. In comparison with the model eye, some reduction is already expected due to microsaccade movements of the eye.

- In the experiments of chapter 3 and chapter 4 we used diode lasers that were available in the laboratory, which did not have the preferable wavelength for DP imaging instruments, and did not emit, when pumped below threshold, the power needed for DP imaging of real eyes. Nowadays many companies manufacture diode lasers with wavelength and output power adapted for specific applications. A thorough search is needed to determine whether lasers that can emit near-infrared light of sufficient power when pumped under the threshold (i.e. hundreds of microwatts to a few milliwatts) are commercially available. If low cost lasers that meet these requirements are found, our results indicate that they can be an all-optical solution for speckle reduction in DP imaging.

- In future work it can also be of interest to map in detail the speckle reduction as a function of the current modulation parameters (pump current dc value, modulation amplitude and frequency) and optical feedback parameters (feedback strength, delay time) and also the camera exposure time.

- Changing the coherence of light from a single light source could be attractive in applications where different imaging modalities are desired. This could be used to switch from a high speckle mode for laser speckle contrast imaging to measure blood flow to a low speckle mode for optical imaging. However, the low speckle mode would offer low intensity.

- It could also be interesting to further investigate whether LD can be tailored through optical feedback-induced or pump current-induced optical chaos in the cavity or specifically designed cavities [86], to emit sufficiently broadband light to reduce speckle in DP images

in a non-mechanical way. Particularly promising is the so-called coherence collapse regime, characterized by an abrupt increase of the line width [38, 81]. However, such sources are not commercially available.

- Sending light through a long multimode fiber reduces speckle due to modal dispersion [62–64]. Possibly this fact could be utilized.
- Another non-mechanical speckle reduction solution that could be applied to DP imaging is the combination of several spectrally separated LDs.

Bibliography

[1] P. Artal, ed. *Handbook of visual optics. Fundamentals and eye optics*. Vol. 1 & 2. CRC Press, 2017.

[2] M. Kaschke, K.-H. Donnerhacke, and M. S. Rill. *Optical Devices in Ophthalmology and Optometry. Technology, Design Principles and Clinical Applications*. Wiley - VCH, 2014.

[3] D. A. Atchison and G. Smith. *Optics of the Human Eye*. Butterworth Heinemann, 2000.

[4] J. Santamaría, P. Artal, and J. Bescós, "Determination of the point-spread function of human eyes using a hybrid optical–digital method", *J. Opt. Soc. Am. A* **4**, 1109 (1987).

[5] P. Artal, S. Marcos, D. R. Williams, and R. Navarro, "Odd aberrations and double-pass measurements of retinal image quality", *J. Opt. Soc. Am. A* **12**, 195 (1995).

[6] P. Artal, D. G. Green, I. Iglesias, and N. López-Gil, "Double-pass measurements of the retinal-image quality with unequal entrance and exit pupil sizes and the reversibility of the eye's optical system", *J. Opt. Soc. Am. A* **12**, 2358 (1995).

[7] J. L. Güell, J. Pujol, M. Arjona, F. Diaz-Douton, and P. Artal, "Optical Quality Analysis System: Instrument for objective clinical evaluation of ocular optical quality", *J. Cataract Refract. Surg.* **30**, 1598 (2004).

[8] J. M. Bueno, G. Pérez, A. Benito, and P. Artal, "Impact of scatter on double-pass image quality and contrast sensitivity measured with a single instrument", *Biomed. Opt. Express* **6**, 4841 (2015).

[9] M. Vinas, C. Dorronsoro, D. Cortes, D. Pascual, and S. Marcos, "Longitudinal chromatic aberration of the human eye in the visible and near infrared from wavefront sensing, double-pass and psychophysics", *Biomed. Opt. Express* **6**, 948 (2015).

[10] J. Zhao, F. Xiao, J. Kang, H. Zhao, Y. Dai, and Y. Zhang, "Quantifying intraocular scatter with near diffraction-limited double-pass point spread function", *Biomed. Opt. Express* **7**, 4595 (2016).

[11] J. Zhao, F. Xiao, H. Zhao, Y. Dai, and Y. Zhang, "Effect of higher-order aberrations and intraocular scatter on contrast sensitivity measured with a single instrument", *Biomed. Opt. Express* **8**, 2138 (2017).

[12] T. T. J. M. Berendschot, P. J. DeLint, and D. van Norren, "Fundus reflectance – historical and present ideas", *Progress in Retinal and Eye Research* **22**, 171 (2003).

[13] J. March i Nogué. *Schematic diagram of the human eye*. 2016. URL: https://en.wikipedia.org/wiki/Fovea_centralis#/media/File:Schematic_diagram_of_the_human_eye_en.svg (visited on 10/11/2019).

[14] F. Díaz-Doutoón, A. Benito, J. Pujol, M. Arjona, J. L. Güell, and P. Artal, "Comparison of the Retinal Image Quality with a Hartmann-Shack Wavefront Sensor and a Double-Pass Instrument", *Investigative Ophthalmology & Visual Science* **47**, 1710 (2006).

[15] J. M. Artigas. *Optica Fisiológica*. 1995.

[16] P. Santos Vives. "Novel system for measuring the scattering of the cornea and the lens". PhD thesis. Universitat Politècnica de Catalunya, 2018.

[17] A. Guirao. "Optical and visual metrics". *Handbook of visual optics*. Ed. by P. Artal. Vol. 2. CRC Press, 2017.

[18] J. A. Martínez-Roda, M. Vilaseca, J. C. Ondategui, A. Giner, F. J. Burgos, G. Cardona, and J. Pujol, "Optical quality and intraocular scattering in a healthy young population", *Clinical and Experimental Optometry* **94**, 223 (2011).

[19] P. Artal, A. Benito, G. M. Pérez, E. Alcón, Á. D. Casas, J. Pujol, and J. M. Marín, "An Objective Scatter Index Based on Double-Pass Retinal Images of a Point Source to Classify Cataracts", *PLOS ONE* **6**, 1 (2011).

[20] International Electrotechnical Commission. *Safety of laser products - Part 1: Equipment classification and requirements (IEC:60825-1:2008)*. Standard. 2008.

[21] J. C. Ondategui, M. Vilaseca, M. Arjona, A. Montasell, G. Cardona, J. L. Güell, and J. Pujol, "Optical quality after myopic photorefractive keratectomy and laser in situ keratomileusis: Comparison using a double-pass system", *J. Cataract Refract. Surg.* **38**, 16 (2012).

[22] M. Vilaseca, M. J. Romero, M. Arjona, S. O. Luque, J. C. Ondategui, A. Salvador, J. L. Güell, P. Artal, and J. Pujol, "Grading nuclear, cortical and posterior subcapsular cataracts using an objective scatter index measured with a double-pass system", *Br. J. Ophthalmol.* **96**, 1204 (2012).

[23] A. Benito, G. M. Pérez, S. Mirabet, M. Vilaseca, J. Pujol, J. M. Marín, and P. Artal, "Objective optical assessment of tear-film quality dynamics in normal and mildly symptomatic dry eyes", *Journal of Cataract & Refractive Surgery* **37**, 1481 (2011).

[24] *Optical quality analysis system (OQAS) by Visiometrics SL, Terrassa, Spain*. URL: http://www.visiometrics.com/ (visited on 10/23/2019).

[25] M. Planck. "Zur Theorie des Gesetzes der Energieverteilung im Normalspectrum". *Verhandlungen der Deutschen Physikalischen Gesellschaft*. Vol. 2. 1900, 237.

[26] A. Einstein, "Über einen die Erzeugung und Verwandlung des Lichtes betreffenden heuristischen Gesichtspunkt", *Annalen der Physik* **322**, 132 (1905).

[27] A. Einstein, "Zur Quantentheorie der Strahlung", *Physikalische Zeitschrift* **18**, 121 (1917).

[28] A. L. Schawlow and C. H. Townes, "Infrared and Optical Masers", *Phys. Rev.* **112**, 1940 (1958).

[29] T. H. Maiman, "Stimulated Optical Radiation in Ruby", *Nature* **187**, 493 (1960).

[30] T. H. Maiman, "Optical and Microwave-Optical Experiments in Ruby", *Phys. Rev. Lett.* **4**, 564 (1960).

[31] S. Bittner, S. Guazzotti, Y. Zeng, X. Hu, H. Yılmaz, K. Kim, S. S. Oh, Q. J. Wang, O. Hess, and H. Cao, "Suppressing spatiotemporal lasing instabilities with wave-chaotic microcavities", *Science* **361**, 1225 (2018).

[32] J. W. Goodman. *Statistical Optics*. 2nd ed. Wiley, 2015.

[33] B. E. A. Saleh and M. C. Teich. *Fundamentals of Photonics*. 1st ed. John Wiley & Sons, Inc., 1991.

[34] R. Lang and K. Kobayashi, "External optical feedback effects on semiconductor injection laser properties", *IEEE Journal of Quantum Electronics* **16**, 347 (1980).

[35] J. Ohtsubo. *Semiconductor Lasers. Stability, Instability and Chaos*. 3rd ed. Vol. 111. Springer, Berlin, Heidelberg, 2013.

[36] D. M. Kane and K. A. Shore, eds. *Unlocking Dynamical Diversity. Optical feedback effects on semiconductor lasers*. John Wiley & Sons, Inc., 2005.

[37] M. C. Soriano, J. García-Ojalvo, C. R. Mirasso, and I. Fischer, "Complex photonics: Dynamics and applications of delay-coupled semiconductors lasers", *Rev. Mod. Phys.* **85**, 421 (2013).

[38] M. Sciamanna and K. A. Shore, "Physics and applications of laser diode chaos", *Nature Photonics* **9**, 151 (2015).

[39] C. A. Quintero Quiroz. "Temporal correlations and dynamical transitions in semiconductor lasers with optical feedback". PhD thesis. Universitat Politècnica de Catalunya, 2017.

[40] R. Tkach and A. Chraplyvy, "Regimes of feedback effects in 1.5-μm distributed feedback lasers", *Journal of Lightwave Technology* **4**, 1655 (1986).

[41] V. Shidlovski. *Superluminescent Diodes. Short overview of device operation principles and performance parameters*. Tech. rep. SuperlumDiodes Ltd., 2004. URL: http://www.superlumdiodes.com/pdf/sld_overview.pdf (visited on 10/10/2019).

[42] J. C. Dainty, A. E. Ennos, M. Françon, J. W. Goodman, T. S. McKechnie, and P. Gareth. *Laser Speckle and Related Phenomena*. Ed. by J. C. Dainty. Springer, 1975.

[43] J. W. Goodman, "Some fundamental properties of speckle", *J. Opt. Soc. Am.* **66**, 1145 (1976).

[44] J. W. Goodman. *Speckle Phenomena in Optics: Theory and Applications*. Roberts & Company, 2007.

[45] D. A. Boas and A. K. Dunn, "Laser speckle contrast imaging in biomedical optics", *Journal of Biomedical Optics* **15**, 1 - 12 (2010).

[46] E. Valent and Y. Silberberg, "Scatterer recognition via analysis of speckle patterns", *Optica* **5**, 204 (2018).

[47] B. Redding, S. M. Popoff, and H. Cao, "All-fiber spectrometer based on speckle pattern reconstruction", *Opt. Express* **21**, 6584 (2013).

[48] B. Redding, S. F. Liew, R. Sarma, and H. Cao, "Compact spectrometer based on a disordered photonic chip", *Nature Photonics* **7**, 746 (2013).

[49] B. Redding and H. Cao, "Using a multimode fiber as a high-resolution, low-loss spectrometer", *Opt. Lett.* **37**, 3384 (2012).

[50] G. D. Bruce, L. O'Donnell, M. Chen, and K. Dholakia, "Overcoming the speckle correlation limit to achieve a fiber wavemeter with attometer resolution", *Opt. Lett.* **44**, 1367 (2019).

[51] P. S. Idell, J. R. Fienup, and R. S. Goodman, "Image synthesis from nonimaged laser-speckle patterns", *Opt. Lett.* **12**, 858 (1987).

[52] J. Bertolotti, E. G. van Putten, C. Blum, A. Lagendijk, W. L. Vos, and A. P. Mosk, "Non-invasive imaging through opaque scattering layers", *Nature* **491**, 232 (2012).

[53] E. Edrei and G. Scarcelli, "Memory-effect based deconvolution microscopy for super-resolution imaging through scattering media", *Scientific Reports* **6**, 33558 (2016).

[54] E. Edrei and G. Scarcelli, "Optical imaging through dynamic turbid media using the Fourier-domain shower-curtain effect", *Optica* **3**, 71 (2016).

[55] O. Katz, E. Small, and Y. Silberberg, "Looking around corners and through thin turbid layers in real time with scattered incoherent light", *Nature Photonics* **6**, 549 (2012).

[56] O. Katz, P. Heidmann, M. Fink, and S. Gigan, "Non-invasive single-shot imaging through scattering layers and around corners via speckle correlations", *Nature Photonics* **8**, 784 (2014).

[57] B. Redding, M. A. Choma, and H. Cao, "Speckle-free laser imaging using random laser illumination", *Nature Photonics* **6**, 355 (2012).

[58] G. Verschaffelt, S. Roelandt, Y. Meuret, W. Van den Broeck, K. Kilpi, B. Lievens, A. Jacobs, P. Janssens, and H. Thienpont, "Speckle disturbance limit in laser-based cinema projection systems", *Scientific Reports* **5**, 14105 (2015).

[59] J. Pauwels and G. Verschaffelt, "Speckle reduction in laser projection using microlens-array screens", *Opt. Express* **25**, 3180 (2017).

[60] T. Stangner, H. Zhang, T. Dahlberg, K. Wiklund, and M. Andersson, "Step-by-step guide to reduce spatial coherence of laser light using a rotating ground glass diffuser", *Appl. Opt.* **56**, 5427 (2017).

[61] B. Dingel and S. Kawata, "Speckle-free image in a laser-diode microscope by using the optical feedback effect", *Opt. Lett.* **18**, 549 (1993).

[62] M. Imai and Y. Ohtsuka, "Speckle-pattern contrast of semiconductor laser propagating in a multimode optical fiber", *Optics Communications* **33**, 4 (1980).

[63] R. Dandliker, A. Bertholds, and F. Maystre, "How modal noise in multimode fibers depends on source spectrum and fiber dispersion", *Journal of Lightwave Technology* **3**, 7 (1985).

[64] J. G. Manni and J. W. Goodman, "Versatile method for achieving 1% speckle contrast in large-venue laser projection displays using a stationary multimode optical fiber", *Opt. Express* **20**, 11288 (2012).

[65] R. Navarro, P. Artal, and D. R. Williams, "Modulation transfer of the human eye as a function of retinal eccentricity", *J. Opt. Soc. Am. A* **10**, 201 (1993).

[66] K. Hampson, S. Chin, and E. Mallen, "Binocular Shack–Hartmann sensor for the human eye", *J. Mod. Opt.* **55**, 703 (2008).

[67] V. Albanis, E. N. Ribak, and Y. Carmon, "Reduction of speckles in retinal reflection", *Appl. Phys. Lett.* **91**, 054104 (2007).

[68] C. García-Guerra, M. Aldaba, M. Arjona, and J. Pujol, "Speckle reduction in double-pass retinal images using variable-focus lenses", *J. Eur. Opt. Soc. Rapid Publ.* **10**, 15001 (2015).

[69] H. Hofer, P. Artal, B. Singer, J. L. Aragón, and D. R. Williams, "Dynamics of the eye's wave aberration", *J. Opt. Soc. Am. A* **18**, 497 (2001).

[70] F. Sanabria, M. A. Arévalo, F. Díaz-Doutón, C. E. García-Guerra, and J. P. Ramo, "Technical improvements applied to a double-pass setup for performance and cost optimization", *Opt. Eng.* **53**, 061710 (2014).

[71] C. E. García Guerra. "Multimodal eye's optical quality (MEOQ)". PhD thesis. Universitat Politècnica de Catalunya, 2016.

[72] S. Marcos and R. Navarro, "Imaging the foveal cones in vivo through ocular speckle interferometry: theory and numerical simulations", *J. Opt. Soc. Am. A* **13**, 2329 (1996).

[73] D. Halpaap, C. E. García-Guerra, M. Vilaseca, and C. Masoller, "Speckle reduction in double-pass retinal images", *Scientific Reports* **9**, 4469 (2019).

[74] S. Marcos, "Image Quality of the Human Eye", *International Ophthalmology Clinics* **43** (2003).

[75] A. Roorda, C. A. Garcia, and J. A. Martin, "What can adaptive optics do for a scanning laser ophthalmoscope?", *Bull. Soc. belge Ophtalmol.* **302**, 231 (2006).

[76] L. N. Thibos, X. Hong, A. Bradley, and X. Cheng, "Statistical variation of aberration structure and image quality in a normal population of healthy eyes", *J. Opt. Soc. Am. A* **19**, 2329 (2002).

[77] P. Artal and R. Navarro, "Monochromatic modulation transfer function of the human eye for different pupil diameters: an analytical expression", *J. Opt. Soc. Am. A* **11**, 246 (1994).

[78] S. Marcos, S. A. Burns, and J. C. He, "Model for cone directionality reflectometric measurements based on scattering", *J. Opt. Soc. Am. A* **15**, 2012 (1998).

[79] R. Legras, A. Gaudric, and K. Woog, "Distribution of cone density, spacing and arrangement in adult healthy retinas with adaptive optics flood illumination", *PLOS ONE* **13**, 1 (2018).

[80] J. B. Jonas, U. Schneider, and G. O. H. Naumann, "Count and density of human retinal photoreceptors", *Graefe's Archive for Clinical and Experimental Ophthalmology* **230**, 505 (1992).

[81] D. Lenstra, B. Verbeek, and A. Den Boef, "Coherence collapse in single-mode semiconductor lasers due to optical feedback", *IEEE Journal of Quantum Electronics* **21**, 674 (1985).

[82] D. Halpaap, J. Tiana-Alsina, M. Vilaseca, and C. Masoller, "Experimental characterization of the speckle pattern at the output of a multimode optical fiber", *Opt. Express* **27**, 27737 (2019).

[83] N. López-Gil and P. Artal, "Comparison of double-pass estimates of the retinal-image quality obtained with green and near-infrared light", *J. Opt. Soc. Am. A* **14**, 961 (1997).

[84] M. Vilaseca and J. Pujol, "Response to the Letter to the Editor by Dr van den Berg", *Clinical and Experimental Optometry* **94**, 393 (2011).

[85] D. Lyon. *Photopic luminosity function*. 2006. URL: https://en.wikipedia.org/wiki/File:Luminosity.svg (visited on 10/24/2019).

[86] B. Redding, A. Cerjan, X. Huang, M. L. Lee, A. D. Stone, M. A. Choma, and H. Cao, "Low spatial coherence electrically pumped semiconductor laser for speckle-free full-field imaging", *Proceedings of the National Academy of Sciences of the United States of America* **112**, 1304 (2015).

[87] K. Kim, S. Bittner, Y. Zeng, S. F. Liew, Q. Wang, and H. Cao, "Electrically pumped semiconductor laser with low spatial coherence and directional emission", *Applied Physics Letters* **115**, 071101 (2019).

[88] H. Cao, R. Chriki, S. Bittner, A. A. Friesem, and N. Davidson, "Complex lasers with controllable coherence", *Nature Reviews Physics* **1**, 156 (2019).

Publications

Journal articles

- Donatus Halpaap, Carlos E. García-Guerra, Meritxell Vilaseca, Cristina Masoller: "Speckle reduction in double-pass retinal images" Scientific Reports 9, 4469 (2019)
- Donatus Halpaap, Jordi Tiana-Alsina, Meritxell Vilaseca, Cristina Masoller: "Experimental characterization of the speckle pattern at the output of a multimode optical fiber" Opt. Express 27, 27737-27744 (2019)

Conference proceedings

- Donatus Halpaap, Meritxell Vilaseca, and Cristina Masoller "Incoherent light sources for speckle reduction in double pass ocular imaging", Proc. SPIE 10416, Optical Coherence Imaging Techniques and Imaging in Scattering Media II, 104160S (1 August 2017)
- Donatus Halpaap, Jordi Tiana-Alsina, Meritxell Vilaseca, and Cristina Masoller "Characterization of speckle patterns generated by a semiconductor laser with optical feedback for speckle reduction in retinal imaging instruments", Proc. SPIE 11078, Optical Coherence Imaging Techniques and Imaging in Scattering Media III, 110782A (19 July 2019)

Additional work not related to this thesis

- Concetta Barcellona, Donatus Halpaap, Pablo Amil, Arturo Buscarino, Jordi Tiana-Alsina and Cristina Masoller: "Remote sensing of audio signals from videos of optical speckle patterns: a comparative study of data processing approaches" (in preparation)

Conferences, schools and workshops

Conference contributions

- European Conferences on Biomedical Optics, München, Germany, 25 – 29 June 2017
  Poster: "Incoherent Light Sources for Speckle Reduction in Double Pass Ocular Imaging"
- International Conference on BioMedical Photonics, La Grande-Motte, France, 17 March 2018
  Poster: "Comparison of Speckle Formation in Double Pass Images with Different Light Sources"
- FisEs XXII Congreso de Física Estadística, Madrid, Spain, 18 – 20 October 2018
  Poster: "Exploiting optical chaos for speckle reduction in double pass ocular imaging"
- VIII Complexitat Day, Barcelona, Spain, 21 May 2019
  Poster: "Statistical properties of speckle patterns in dependence of laser parameters and image acquisition time"
- European Conference on Biomedical Optics, München, Germany, 23 – 26 June 2019
  Poster: "Characterization of speckle patterns generated by a semiconductor laser with optical feedback for speckle reduction in retinal imaging instruments"

School and workshop participations

- Siegman International School on Lasers, Castelldefels, Spain, 24 – 29 July 2016
- 1st BE-OPTICAL School: Fundamentals of Biophotonics, Imaging, and Cardiac Electrophysiology, Göttingen, Germany, 14 – 18 November 2017
  Oral presentation: "Speckle Reduction in Double Pass Ocular Imaging"
- Jornada d'Investigadors Predoctorals Interdisciplinària, Barcelona, Spain, 9 February 2017
  Poster: "Incoherent Light Sources for Speckle Reduction in Double Pass Ocular Imaging"
- 3rd ESASO Anterior Segment Academy, Instituto de Microcirugía Ocular, Barcelona, Spain, 21 – 22 April 2017

- 2nd BE-OPTICAL School, Toruń, Poland, 02 – 05 May 2017
  Oral presentation: "Incoherent Light Sources for Speckle Reduction in Double Pass Ocular Imaging"

- BE-OPTICAL Mid-Term Review Meeting & 1st BE-OPTICAL Workshop, Alcúdia, Spain, 25 September 2017
  Oral presentation and poster: "Incoherent Light Sources for Speckle Reduction in Double Pass Ocular Imaging"

- 2nd BE-OPTICAL Workshop, La Grande-Motte, France, 19 March 2018
  Oral presentation and poster: "Speckle Quantification in Double Pass Images of Real Eyes"

- BioPhysics By The Sea Workshop & 3rd BE-OPTICAL Workshop, Alcúdia, Spain, 7 – 12 October 2018
  Oral presentation: "Exploring different speckle reduction techniques for double pass ocular imaging"

- XIV Research Meeting of the Department of Physics, Barcelona, Spain, 29 January 2019
  Poster: "Exploiting optical chaos for speckle reduction in double pass ocular imaging"

- Jornada d'Investigadors Predoctorals Interdisciplinària, Barcelona, Spain, 4 February 2019
  Poster presentation: "Exploiting optical chaos for speckle reduction in double pass ocular imaging"

- 4th BE-OPTICAL Workshop, Berlin, Germany, 4 – 12 March 2019
  Oral presentation: "Speckle contrast measurements in dependence of laser diode pump current"

- BE-OPTICAL final conference: New trends in biomedical imaging and data analysis, Göttingen, Germany, 3 – 4 July 2019
  Oral presentation: "Experimental characterization of the speckle pattern at the output of a multimode optical fiber"